HAL
archives-ouvertes.fr

Ionic Parameters Estimation in Multi-Scale Cardiac Electrophysiology Modelling

Yassine Abidi, Moncef Mahjoub, Nejib Zemzemi

▶ To cite this version:

IONIC PARAMETERS ESTIMATION IN MULTI-SCALE CARDIAC ELECTROPHYSIOLOGY MODELLING

YASSINE ABIDI[1], MONCEF MAHJOUB[1] AND NÉJIB ZEMZEMI[2]

ABSTRACT. In this work, we present an optimal control formulation for the bidomain model in order to estimate maximal conductance parameters in cardiac electrophysiology multiscale modelling. We consider a general Hodgkin-Huxley formalism to describe the ionic exchanges at the microscopic level. We treat the desired parameters as control variables in a cost function minimizing the gap between the measured and the computed transmembrane potentials. First, we establish the existence of an optimal control solution and we formally derive the optimality system. Second, we propose a strategy for solving the estimation problem for both single and multiple parameters cases. Our algorithm is based on a gradient descent method, where the gradient is obtained by solving an adjoint problem. Both the state and the adjoint problems are solved using the finite element method. Numerical simulations for single and multiple conductances estimations show the capability of this approach to identify the values of sodium, calcium and potassium ion channels conductances of the Luo Rudy phase I model.

Keywords: Optimal control with PDE constraints, bidomain model, physiological ionic model, maximal conductance parameters.

1. INTRODUCTION

In the last decades, the mathematical modelling of cardiac electrical activity has been recognized as one of the potential approaches capable of revealing diagnostic information about the heart. The electrical behavior of the cardiac tissue is described by a system consisting of partial differential equations (PDEs) coupled to a system of ordinary differential equations (ODEs) modelling the transmbrane ionic exchanges at the microscopic level. The model of the cell membrane dynamics is expressed using the Hodgkin-Huxley (HH) formalism [28]. This model was adapted by Denis Nobel for Purkinje heart cells [38]. Since that, several other models have been introduced to describe the electrical activity of the cell membrane in the myocardium. Beeler and Reuter [8] introduced the model for ventricular cells. Later, Di Francesco and Noble [25] proposed a model that considers ion pumps, which allows different chemical species such as potassium, sodium and calcium to return to their stable state. Moreover, a family of more complex models based always on the HH formalism taking into account the physiological behavior of the ion channels [34, 35, 29, 42, 26] have been proposed in the litterature. In all these models, maximal conductances play an important role in the generation of the electrical potential, the determination of some pathological conditions or in the study of the effect of drugs. Several authors investigated the optimization of parameters or source terms in the mathematical model of cardiac electrophysiology. Brandao et al. [13] studied the theoretical analysis and the controllability of the optimization subject to the FitzHugh-Nagumo model. Later, systematic analysis and numerical studies for the optimal control of monodomain and bidomain model are presented in [16, 4, 14, 31, 17, 7, 18], and more recently for the optimal control of bidomain-bath model using Mitchell-Shaeffer model in 3D geometries [19, 9, 15]. In [21, 40, 41] authors established an experimental estimation of the intracellular and extracellular conductivities. Yan and Veneziani [46] use a variational procedure for the estimation of cardiac conductivities from measures of the transmembrane and extracellular potentials

available at some sites of the tissue. Beretta et al. [10] define a numerical reconstruction procedure for the inverse problem of detecting a spherical inhomogeneity from boundary measurements of the electric potential. Moreover, the identification from measurements of surface potentials has been tackled in an optimization framework for numerical purposes [6, 20, 37]. In an other work [36], authors propose a strategy to optimize a non differentiable cost function obtained from a fit of activation times map. Recently, the identification of the maximal conductances has been subject of theoretical studies in the monodomain [1, 11, 5, 32] and bidomain [45, 2] models. In an other work [12], authors propose a numerical approach for the analysis of drugs effects on the electrical activity of hiPSC-CMs based on multi-electrode array experiments where the drug acts directly on the maximal conductance of the targeted ion channel. In our work, we still use a variational procedure for the estimation of a set of ionic maximal conductances by an optimal control approach. This approach is based on the minimization of an appropriate cost functional that depends on the maximal conductances and a measures of the transmembrane potential.

The paper is organized as follows: In Section 2, we briefly recall the bidomain model and the general structure of cardiac cellular membrane models describing the electrical wave propagation and the ionic exchange at the cell membrane respectively. We also present some preliminary material, including relevant notations, assumptions and regularities. Section 3 is devoted to the optimal control problem. We prove the existence of the control and we provide a formal derivation of the adjoint equations and the first order optimality condition, which are the basis for numerical resolution. The description of the numerical approach to solve the primal and the adjoint state equations and the optimization problem are explained in section 4. Finally, in Section 5, numerical results are presented for the different test cases. A summary and concluding remarks are given then in the last section.

2. MATHEMATICAL MODEL

Let $\Omega \subset \mathbb{R}^d$ $(d \geqslant 1)$ be a bounded connected open set whose boundary $\Gamma = \partial\Omega$ is regular enough, $(\Omega \subset \mathbb{R}^3$ being the natural domain of the hearth). Let $T > 0$ be a fixed time horizon. We will use the notation $Q = \Omega \times (0, T)$, and $\Sigma = \Gamma \times (0, T)$.

We introduce a parabolic-elliptic system called *bidomain model*, coupled to a system of ODEs. This model was proposed in the late 1970s by Tung [43] and is now the generally accepted model of electrical behaviour of cardiac tissue (see Henriquez [27], Keener and Sneyd [30]), can be written as:

$$(2.1) \quad \begin{cases} A_m\big(C_m\partial_t v + I_{ion}(\bar{\boldsymbol{\varrho}}, v, \mathbf{w}, \mathbf{z})\big) - div(\boldsymbol{\sigma}_i\nabla v) = div(\boldsymbol{\sigma}_i\nabla u_e) + A_m I_{app} & \text{in } Q, \\ -div(\boldsymbol{\sigma}_i\nabla v + (\boldsymbol{\sigma}_i + \boldsymbol{\sigma}_e)\nabla u_e) = 0 & \text{in } Q, \\ \partial_t\mathbf{w} = \boldsymbol{F}(v, \mathbf{w}) & \text{in } Q, \\ \partial_t\mathbf{z} = \boldsymbol{G}(\bar{\boldsymbol{\varrho}}, v, \mathbf{w}, \mathbf{z}) & \text{in } Q, \\ \boldsymbol{\sigma}_i\nabla v.\nu + \boldsymbol{\sigma}_i\nabla u_e.\nu = 0 & \text{on } \Sigma, \\ \boldsymbol{\sigma}_i\nabla v.\nu + (\boldsymbol{\sigma}_i + \boldsymbol{\sigma}_e)\nabla u_e.\nu = 0 & \text{on } \Sigma, \\ v(x, 0) = v_0(x), \quad \mathbf{w}(x, 0) = \mathbf{w}_0(x), \quad \mathbf{z}(x, 0) = \mathbf{z}_0(x) & \text{in } \Omega, \end{cases}$$

where $v : Q \to \mathbb{R}$ is the transmembrane potential, $u_e : Q \to \mathbb{R}$ is the extracellular electric potential, and $\boldsymbol{\sigma}_i, \boldsymbol{\sigma}_e : \Omega \to \mathbb{R}^{d \times d}$ are respectively the intra- and extracellular conductivity tensors. $\mathbf{w} : Q \to \mathbb{R}^k$ represent the gating variables and $\mathbf{z} : Q \to \mathbb{R}^m$ are the ionic intracellular concentration variables. A_m is the surface to volume ratio of the cardiac cells, and $C_m > 0$ is the membrane capacitance per unit area. $I_{app} : Q \to \mathbb{R}$ is the applied current source and $\bar{\boldsymbol{\varrho}} := \{\bar{\varrho}_i\}_{1 \leqslant i \leqslant N}$ represent a set of maximal conductance parameters. The I_{ion} is the current density flowing through the ionic channels and the functions $\boldsymbol{F}$ and $\boldsymbol{G}$ determine the evolution of the gating variables and intracellular concentrations, respectively, they are

determined by an electrophysiological cell model. In an isolated heart conditions, no current flows out of the heart as expressed by the homogeneous Neumann boundary conditions. We denote by ν the unit normal to Γ outward of Ω.

2.1. **Membrane models and ionic currents.** Following work by Hodgkin and Huxley [28], many HH-based models have later been developed for the cardiac action potential. In these models, the ionic current I_{ion} through channels of the membrane, has the following general structure [39]:

$$(2.2) \qquad I_{ion}(\bar{\boldsymbol{\varrho}}, v, \mathbf{w}, \mathbf{z}) = \sum_{i=1}^{N} \bar{\varrho}_i y_i(v) \prod_{j=1}^{k} w_j^{p_{j,i}} (v - E_i(\mathbf{z})),$$

where N is the number of ionic currents, $\bar{\varrho}_i := \bar{\varrho}_i(x)$ is the maximal conductance associated with the ith current, y_i is a gating function depending only on the membrane potentiel v, $p_{j,i}$ are positive integers exponents and E_i is the reversal potential for the ith current, which is given by Godman-Hodgkin-Katz (GHK) equation:

$$(2.3) \qquad E_i = \frac{RT}{F} \ln \left(\frac{\sum_j PR_{X_j^+}[X_j^+]_{out} + \sum_k PR_{X_k^-}[X_k^-]_{in}}{\sum_j PR_{X_j^+}[X_j^+]_{in} + \sum_k PR_{X_k^-}[X_k^-]_{out}} \right),$$

where R, T and F designate, respectively, the perfect gas constant, the temperature and the Faraday constant. $PR_{X_{j,k}^{\pm}}$ represents the permeability for the ion $X_{j,k}^{\pm}$, and $[X_{j,k}^{\pm}]_{in}$ (respectively $[X_{j,k}^{\pm}]_{out}$) is the intracellular (respectively extracellular) concentration of the ion $X_{j,k}^{\pm}$. We recall that GHK equation is a generalized form of the Nernst equation.

For the ODEs, the dynamics of the gating variable $\mathbf{w}$ is described in the HH formalism by a system of ordinary differential equations which when w_j is a gating variable ($0 \leqslant w_j \leqslant 1$) are governed by the following equation:

$$(2.4) \qquad \partial_t w_j = F_j(v, w_j) := \alpha_j(v)(1 - w_j) - \beta_j(v)w_j, \quad j = 1, \ldots, k,$$

where α_j and β_j two positive rational functions of exponentials in v. A general expression for both α_j and β_j is given by

$$(2.5) \qquad \frac{C_1 \exp[C_2(v + C_3)] + C_4(v + C_5)}{\exp[C_5(v + C_3)] + C_7},$$

where $C_1, C_2, \ldots, C_7$ are constants. For the dynamics of the ionic concentration variables $\mathbf{z}$, we have the system of ODE's:

$$(2.6) \qquad \partial_t z_i = G_i(\bar{\boldsymbol{\varrho}}, v, \mathbf{w}, \mathbf{z}) := -J_i(\bar{\boldsymbol{\varrho}}, v, \mathbf{w}, \log z_i) + H_i(\bar{\boldsymbol{\varrho}}, v, \mathbf{w}, \mathbf{z}), \quad i = 1, \ldots, m.$$

where the functions J_i and H_i are described in the Assumptions 2.1.

2.2. **Conductivity tensors.** The anisotropic properties of the two media are modeled by an intracellular and extracellular conductivity tensors $\boldsymbol{\sigma}_i(x)$ and $\boldsymbol{\sigma}_e(x)$. Generally, the conductivities $\boldsymbol{\sigma}_i$ and $\boldsymbol{\sigma}_e$ are two matrices given by

$$\boldsymbol{\sigma}_j(x) = \sigma_j^t(x)\boldsymbol{I} + (\sigma_j^l(x) - \sigma_j^t(x))\boldsymbol{a}_l(x)\boldsymbol{a}_l^T(x),$$

where σ_j^l and σ_j^t, $j \in \{i, e\}$ denote the intra- and extracellular conductivities along and transversal to the direction of the fiber (parallel to $\boldsymbol{a}_l(x)$), respectively, and $\boldsymbol{I}$ is the identity matrix.

Assumptions 2.1. *(Stronger assumptions on the data in 2.1) We assume that:*

(1) $\Omega \subset \mathbb{R}^3$ is a bounded domain with $C^{1,1}$-boundary.

(2) $\boldsymbol{\sigma}_i, \boldsymbol{\sigma}_e : \bar{\Omega} \to \mathbb{R}^{3\times 3}$ *are symmetric, positive definite matrix functions with $W^{1,\infty}(\Omega)$-coefficients, obeying the uniform ellipticity conditions:*

$$(2.7) \qquad 0 \leqslant \mu_1 \|\xi\|^2 \leqslant \xi^T \boldsymbol{\sigma}_{i,e}(x)\xi \leqslant \mu_2 \|\xi\|^2, \quad \forall \xi \in \mathbb{R}^3, \ \forall x \in \Omega, \ with \ \mu_1, \mu_2 > 0.$$

(3) *We use the regularized form of the variable $y_i(v)$ in hyperbolic functions introduced in [22]. In this case, $y_i(v)$ is a $\mathcal{C}^\infty$ function with respect to the variable v for $i = 1,\ldots,N$, and then is locally Lipschitz since v is bounded, similarly for the function $v \mapsto y_i(v)v$.*

(4) *J_i and H_i are locally Lipschitz continuous functions where:*

$$(2.8) \quad J_i \in \mathcal{C}^2(\mathbb{R}_+^* \times \mathbb{R} \times \mathbb{R}^k \times \mathbb{R}), \quad 0 < g_*(\mathbf{w}) \leqslant \frac{\partial J_i}{\partial \tau}(\bar{\varrho}, v, \mathbf{w}, \tau) \leqslant g^*(\mathbf{w}), \quad \left|\frac{\partial J_i}{\partial v}(\bar{\varrho}, v, \mathbf{w}, 0)\right| \leqslant L_v(\mathbf{w}),$$

g_*, g^*, L_v *belong to $\mathcal{C}^1(\mathbb{R}^k, \mathbb{R}_+)$, and*

$$(2.9) \qquad H_i \in \mathcal{C}^2(\mathbb{R}_+^* \times \mathbb{R} \times \mathbb{R}^k \times (0, +\infty)^m) \cap \mathrm{Lip}(\mathbb{R}_+^* \times \mathbb{R} \times [0,1]^k \times (0, +\infty)^m).$$

(5) *The intial values belong to the following spaces: $v_0 \in H^2(\Omega), \mathbf{w}_0 \in L^2(\Omega)^k$, and $\mathbf{z}_0 \in L^2(\Omega)^m$, with $\log \mathbf{z}_0 := (\log z_{0,1}, \ldots, \log z_{0,m}) \in L^2(\Omega)^m$. Moreover, v_0 satisfies the compatibility condition described in [44].*

(6) *The extracellular potential u_e has zero average on Ω, i.e $\int_\Omega u_e dx = 0$.*

(7) *I_{app} verifies the compatibility condition: $\int_\Omega I_{app}(x,t)dx = 0, \ \forall t \in (0,T)$.*

Under the assumptions (2.1), the existence and uniqueness of the bidomain model 2.1 for more general physiological ionic models based on the classical Hodgkin-Huxley formalism can be found in [44].

In our numerical computations, we consider the physiological Luo-Rudy phase I model (LR1) [34], which consists of 6 ionic currents:

$$(2.10) \qquad I_{ion} = I_{Na} + I_{si} + I_K + I_{K1} + I_{Kp} + I_b,$$

which are fast sodium current (I_{Na}), slow inward calcium current (I_{si}), time dependent potassium current (I_K), time independent potassium current (I_{K1}), plateau potassium current (I_{Kp}) and background current (I_b). The time dependent currents I_{Na}, I_{si} and I_K, depend on six activation and inactivation gates m, h, j, d, f, x, and one intracellular concentration variable of Calcium $[Ca^{2+}]_i$, which are governed by ODEs of the form:

$$(2.11) \quad \begin{aligned} \frac{dw}{dt} &= \alpha_w(v)(1-w) - \beta_w(v)w, \quad \text{for } w = m, h, j, d, f, x, \\ \frac{d}{dt}[Ca^{2+}]_i &= -10^{-4} I_{si} + 0.07(10^{-4} - [Ca^{2+}]_i), \end{aligned}$$

For details on formulation of those functions and the parameters used in our computations, we refer to the original paper of LR1 model [34].

3. OPTIMAL CONTROL PROBLEM

In this section, we set the optimal control problem, for which the numerical experiments were carried out. Suppose that v_{meas} is the desired state solution at the cardiac domain, we look for the set of parameters $\bar{\boldsymbol{\varrho}} := \{\bar{\varrho}_i\}_{1\leqslant i\leqslant N}$ that solves the following minimization problem:

$$(3.1) \qquad (\mathcal{P}) \begin{cases} \min_{\bar{\boldsymbol{\varrho}} \in \mathcal{C}_{ad}} \mathcal{I}(\bar{\boldsymbol{\varrho}}) = \frac{1}{2}\Big(\epsilon_1 \int_Q |v(\bar{\boldsymbol{\varrho}}) - v_{meas}|^2 \, dxt + \epsilon_2 \int_\Omega |\bar{\boldsymbol{\varrho}}|^2 \, dx\Big), \\ \text{subject to the coupled PDE system (2.1), and } \bar{\boldsymbol{\varrho}} \in \mathcal{C}_{ad}, \end{cases}$$

where $\mathcal{I}$ is the quantity of interest, ϵ_1, ϵ_2 are the regularization parameters and v is the state variable. In addition, a Tikhonov-like regularization term $\int_\Omega |\bar{\varrho}|^2 \, dx$ used to weigh the impact of the regularization in the minimize procedure. $\mathcal{C}_{ad}$ is the admissible domain for control given by

$$(3.2) \qquad \mathcal{C}_{ad} = \{\bar{\varrho} \in L^\infty(\Omega)^N : \; \bar{\varrho}(x) \in [m, M]^N, \; \forall x \in \Omega\}.$$

3.1. Optimal conditions and dual problem.
In this subsection, we formally derive the optimality system associated to (3.1). Let's denote by $\mathcal{J}$ the cost function

$$\mathcal{J}(v, \bar{\varrho}) = \frac{1}{2}\Big(\epsilon_1 \int_Q |v - v_{meas}|^2 \, dxt + \epsilon_2 \int_\Omega |\bar{\varrho}|^2 \, dx\Big).$$

If $v(\bar{\varrho})$ is a solution of (2.1), then we immediately have $\mathcal{J}(v(\bar{\varrho}), \bar{\varrho}) = \mathcal{I}(\bar{\varrho})$. We follow a Lagrangian approach and introduce the Lagrange functional:

$$(3.3) \qquad \mathcal{L}(v, u_e, \mathbf{w}, \mathbf{z}, \bar{\varrho}, \lambda^*) = \mathcal{J}(v, \bar{\varrho}) - \lambda^* \mathcal{S}(v, u_e, \mathbf{w}, \mathbf{z}, \bar{\varrho}),$$

where $\lambda^* := (p, q, \boldsymbol{r}, \boldsymbol{s})(x, t)$ denote the Lagrange multipliers, and $\mathcal{S}(v, u_e, \mathbf{w}, \mathbf{z}, \bar{\varrho})$ is the state equation. Then,

$$
\begin{aligned}
\mathcal{L}(v, u_e, \mathbf{w}, \mathbf{z}, \bar{\varrho}, \lambda^*) \quad &= \mathcal{J}(v, \bar{\varrho}) - \int_Q pA_m\big(C_m\partial_t v + I_{ion}(\bar{\varrho}, v, \mathbf{w}, \mathbf{z}) - I_{app}\big)dxdt \\
&\quad - \int_Q p\big(-div(\boldsymbol{\sigma}_i \nabla v) - div(\boldsymbol{\sigma}_i \nabla u_e)\big)dxdt \\
&\quad - \int_Q q\big(-div(\boldsymbol{\sigma}_i \nabla v + (\boldsymbol{\sigma}_i + \boldsymbol{\sigma}_e)\nabla u_e)\big)dxdt \\
&\quad - \int_Q \boldsymbol{r}.\big(\partial_t\mathbf{w} - \boldsymbol{F}(v, \mathbf{w})\big)dxdt - \int_Q \boldsymbol{s}.\big(\partial_t\mathbf{z} - \boldsymbol{G}(\bar{\varrho}, v, \mathbf{w}, \mathbf{z})\big)dxdt,
\end{aligned}
$$

(3.4)

The first order optimality system is given by the Karusch-Kuhn-Tucker (KKT) conditions which result from equating the partial derivatives of $\mathcal{L}$ with respect to $v, u_e, \mathbf{w}$ and $\mathbf{z}$ equal to zero. First, invoking integration by parts with respect to the temporal variable and Green's formula with respect to the spatial variable, we observe that

$$
\begin{aligned}
(3.5) \qquad < \frac{\partial\mathcal{L}}{\partial v}, \delta v > \quad &= < \frac{\partial\mathcal{J}}{\partial v}, \delta v > -\lambda^* < \frac{\partial\mathcal{S}}{\partial v}, \delta v > \\
&= < \frac{\partial\mathcal{J}}{\partial v}, \delta v > + \int_Q \{A_m(C_m\partial_t p - p\partial_v I_{ion}) + \boldsymbol{r}.\partial_v\boldsymbol{F} + \boldsymbol{s}.\partial_v\boldsymbol{G}\}\delta vdxdt \\
&\quad + \int_Q \{div(\boldsymbol{\sigma}_i \nabla p) + div(\boldsymbol{\sigma}_i \nabla q)\}\delta vdxdt - \int_\Sigma \{\boldsymbol{\sigma}_i \nabla p.\nu + \boldsymbol{\sigma}_i \nabla q.\nu\}\delta vdSdt,
\end{aligned}
$$

$$
\begin{aligned}
(3.6) \qquad < \frac{\partial\mathcal{L}}{\partial u_e}, \delta u_e > \quad &= < \frac{\partial\mathcal{J}}{\partial u_e}, \delta u_e > -\lambda^* < \frac{\partial\mathcal{S}}{\partial u_e}, \delta u_e > \\
&= < \frac{\partial\mathcal{J}}{\partial u_e}, \delta u_e > + \int_Q \{div(\boldsymbol{\sigma}_i \nabla p) + div((\boldsymbol{\sigma}_i + \boldsymbol{\sigma}_e)\nabla q)\}\delta u_e dxdt \\
&\quad - \int_\Sigma \{\boldsymbol{\sigma}_i \nabla p.\nu + (\boldsymbol{\sigma_i} + \boldsymbol{\sigma_e})\nabla q.\nu\}\delta u_e dSdt.
\end{aligned}
$$

$$
\begin{aligned}
(3.7) \qquad < \frac{\partial\mathcal{L}}{\partial \mathbf{w}}, \delta\mathbf{w} > \quad &= < \frac{\partial\mathcal{J}}{\partial \mathbf{w}}, \delta\mathbf{w} > -\lambda^* < \frac{\partial\mathcal{S}}{\partial \mathbf{w}}, \delta\mathbf{w} > \\
&= < \frac{\partial\mathcal{J}}{\partial \mathbf{w}}, \delta\mathbf{w} > + \int_Q \{\partial_t\boldsymbol{r} - A_m p\partial_\mathbf{w} I_{ion} + (\partial_\mathbf{w}\boldsymbol{F})^T\boldsymbol{r} + (\partial_\mathbf{w}\boldsymbol{G})^T\boldsymbol{s}\}.\delta\mathbf{w}dxdt,
\end{aligned}
$$

and

$$(3.8) \quad \begin{aligned} < \frac{\partial \mathcal{L}}{\partial \mathbf{z}}, \delta \mathbf{z} > \quad &=< \frac{\partial \mathcal{J}}{\partial \mathbf{z}}, \delta \mathbf{z} > -\lambda^* < \frac{\partial \mathcal{S}}{\partial \mathbf{z}}, \delta \mathbf{z} > \\ &=< \frac{\partial \mathcal{J}}{\partial \mathbf{z}}, \delta \mathbf{z} > + \int_Q \{\partial_t \boldsymbol{s} - A_m p \partial_{\mathbf{z}} I_{ion} + (\partial_{\mathbf{z}} \boldsymbol{G})^T \boldsymbol{s}\}.\delta \mathbf{z} dx dt. \end{aligned}$$

Herein, we impose the terminal conditions

$$(3.9) \quad p(x,T) = 0, \quad \boldsymbol{r}(x,T) = \boldsymbol{0}, \quad \text{and } \boldsymbol{s}(x,T) = \boldsymbol{0} \text{ in } \Omega,$$

Collecting the previous results with the derivatives of $\mathcal{J}$, we get the following adjoint problem:

$$(3.10) \quad \begin{cases} -A_m(C_m \partial_t p - p \partial_v I_{ion}) - div(\boldsymbol{\sigma}_i \nabla p) - div(\boldsymbol{\sigma}_i \nabla q) - (\partial_v \boldsymbol{F})^T \boldsymbol{r} \\ \qquad -(\partial_v \boldsymbol{G})^T \boldsymbol{s} = \epsilon_1(v - v_{meas}), & \text{in } Q, \\ -div(\boldsymbol{\sigma}_i \nabla p + (\boldsymbol{\sigma}_i + \boldsymbol{\sigma}_e)\nabla q) = 0 & \text{in } Q, \\ -\partial_t \boldsymbol{r} + A_m p \partial_{\mathbf{w}} I_{ion} - (\partial_{\mathbf{w}} \boldsymbol{F})^T \boldsymbol{r} - (\partial_{\mathbf{w}} \boldsymbol{G})^T \boldsymbol{s} = 0 & \text{in } Q, \\ -\partial_t \boldsymbol{s} + A_m p \partial_{\mathbf{z}} I_{ion} - (\partial_{\mathbf{z}} \boldsymbol{G})^T \boldsymbol{s} = 0 & \text{in } Q, \\ p(x,T) = 0, \quad \boldsymbol{r}(x,T) = \boldsymbol{0}, \quad \text{and } \boldsymbol{s}(x,T) = \boldsymbol{0}, & \text{in } \Omega, \end{cases}$$

with the boundary conditions for the adjoint states

$$(3.11) \quad \begin{cases} -\boldsymbol{\sigma}_i \nabla p.\nu - \boldsymbol{\sigma}_i \nabla q.\nu = 0, & \text{on } \Sigma, \\ -\boldsymbol{\sigma}_i \nabla p.\nu - (\boldsymbol{\sigma_i} + \boldsymbol{\sigma_e})\nabla q.\nu = 0 & \text{on } \Sigma, \end{cases}$$

and in addition the zero mean condition:

$$(3.12) \quad \int_\Omega q(t)dx = 0 \text{ holds for a.e. } t \in (0,T).$$

Based on the adjoint equations, to find the optimal conditions, we need to totally differentiate this functional $\mathcal{J}(v, \bar{\boldsymbol{\varrho}})$ with respect to the control variable $\bar{\boldsymbol{\varrho}}$. In addition, the state equation $\mathcal{S}(v, u_e, \mathbf{w}, \mathbf{z}, \bar{\boldsymbol{\varrho}}) = 0$ yields the sensitivity equation:

$$(3.13) \quad \frac{\partial \mathcal{S}}{\partial \bar{\boldsymbol{\varrho}}} + \frac{\partial \mathcal{S}}{\partial \boldsymbol{u}} \frac{d\boldsymbol{u}}{d\bar{\boldsymbol{\varrho}}} = \boldsymbol{0},$$

where $\boldsymbol{u}$ is the state variable. Eventually, using the Gâteaux derivatives of $\mathcal{J}$ as follows:

$$(3.14) \quad \frac{\mathcal{D}\mathcal{J}}{\mathcal{D}\bar{\boldsymbol{\varrho}}} = \frac{\partial \mathcal{J}}{\partial \bar{\boldsymbol{\varrho}}} + \frac{\partial \mathcal{J}}{\partial \boldsymbol{u}} \frac{d\boldsymbol{u}}{d\bar{\boldsymbol{\varrho}}}.$$

Using (3.13) and the adjoint equation $\dfrac{\partial \mathcal{L}}{\partial \boldsymbol{u}} = \dfrac{\partial \mathcal{J}}{\partial \boldsymbol{u}} - \lambda^* \dfrac{\partial \mathcal{S}}{\partial \boldsymbol{u}} = 0$, we get

$$(3.15) \quad \frac{\mathcal{D}\mathcal{J}}{\mathcal{D}\bar{\boldsymbol{\varrho}}} = \frac{\partial \mathcal{J}}{\partial \bar{\boldsymbol{\varrho}}} + \lambda^* \frac{\partial \mathcal{S}}{\partial \boldsymbol{u}} \frac{d\boldsymbol{u}}{d\bar{\boldsymbol{\varrho}}} = \frac{\partial \mathcal{J}}{\partial \bar{\boldsymbol{\varrho}}} - \lambda^* \frac{\partial \mathcal{S}}{\partial \bar{\boldsymbol{\varrho}}} = \frac{\partial \mathcal{L}}{\partial \bar{\boldsymbol{\varrho}}}.$$

Then, we have

$$(3.16) \quad < \frac{\mathcal{D}\mathcal{J}}{\mathcal{D}\bar{\boldsymbol{\varrho}}}, \delta\bar{\boldsymbol{\varrho}} >=< \frac{\partial \mathcal{L}}{\partial \bar{\boldsymbol{\varrho}}}, \delta\bar{\boldsymbol{\varrho}} >= \epsilon_2 \int_\Omega \bar{\boldsymbol{\varrho}}.\delta\bar{\boldsymbol{\varrho}} dx - \int_Q A_m p \frac{\partial}{\partial \bar{\boldsymbol{\varrho}}} I_{ion}.\delta\bar{\boldsymbol{\varrho}} dx dt + \int_Q (\frac{\partial \boldsymbol{G}}{\partial \bar{\boldsymbol{\varrho}}})^T \boldsymbol{s}.\delta\bar{\boldsymbol{\varrho}} dx dt,$$

where $(\frac{\partial \boldsymbol{G}}{\partial \bar{\boldsymbol{\varrho}}})^T$ denotes the transpose of the Jacobian matrix of $\boldsymbol{G} \in \mathbb{R}^m$ in point $\bar{\boldsymbol{\varrho}} \in \mathbb{R}^N$. We deduce the optimality condition of the optimal control problem (3.1):

$$(3.17) \qquad \frac{\mathcal{D}\mathcal{J}}{\mathcal{D}\bar{\boldsymbol{\varrho}}} = \mathbf{0}_{\mathbb{R}^N} \quad \Rightarrow \quad \epsilon_2 \bar{\boldsymbol{\varrho}} - A_m \int_0^T p \frac{\partial}{\partial \bar{\boldsymbol{\varrho}}} I_{ion} dt + \int_0^T (\frac{\partial \boldsymbol{G}}{\partial \bar{\boldsymbol{\varrho}}})^T \boldsymbol{s} dt = \mathbf{0}_{\mathbb{R}^N}, \quad \forall x \in \Omega.$$

3.2. **Existence of the control.** In the following theorem, we show that our optimal control problem (3.1) has a unique solution.

Theorem 3.1. *Under the previous Assumptions 2.1, there exists at least one solution $\bar{\boldsymbol{\varrho}}^*$ of the optimal control problem (3.1).*

Proof. The goal is to prove that there exists $\bar{\boldsymbol{\varrho}}^*$ such that $\mathcal{J}(\bar{\boldsymbol{\varrho}}^*) = \inf\limits_{\bar{\boldsymbol{\varrho}} \in \mathcal{C}_{ad}} \mathcal{J}(\bar{\boldsymbol{\varrho}})$.

Since the cost functional $\mathcal{J} : \mathcal{C}_{ad} \to \mathbb{R}$ is bounded from below, with the admissible domain $\mathcal{C}_{ad}$ (3.2) is a closed and convex non-empty subset of the Banach space $L^\infty(\Omega)^N$, and $\mathcal{J}$ is coercive verifying the property:

$$(3.18) \qquad \forall(\bar{\boldsymbol{\varrho}}^{(k)})_{k\in\mathbb{N}} \in \mathcal{C}_{ad}^\mathbb{N}, \ \lim_{k\to\infty} \left|\bar{\boldsymbol{\varrho}}^{(k)}\right| = +\infty \quad \Rightarrow \quad \lim_{k\to\infty} \mathcal{J}(\bar{\boldsymbol{\varrho}}^{(k)}) = +\infty,$$

Then, there exists a bounded minimining sequence $\bar{\boldsymbol{\varrho}}^{(k)} \in \mathcal{C}_{ad}^\mathbb{N}$ such that

$$(3.19) \qquad \lim_{k\to\infty} \mathcal{J}(\bar{\boldsymbol{\varrho}}^{(k)}) = \inf_{\bar{\boldsymbol{\varrho}} \in \mathcal{C}_{ad}} \mathcal{J}(\bar{\boldsymbol{\varrho}}).$$

Since $L^\infty(\Omega)^N$ is a non-reflexive space, it follows from the sequential Banach-Alaoglu theorem that there exists a subsequence of $\bar{\boldsymbol{\varrho}}^{(k)}$, which we denote by the same symbol, such that

$$(3.20) \qquad \bar{\boldsymbol{\varrho}}^{(k)} \rightharpoonup \bar{\boldsymbol{\varrho}}^* \text{ weakly-* in } L^\infty(\Omega)^N.$$

Let $(v^{(k)}, u_e^{(k)}, \mathbf{w}^{(k)}, \mathbf{z}^{(k)})$ be the associated solution of the bidomain model (2.1) with $\bar{\boldsymbol{\varrho}}^{(k)}$, by the weak compactness property, see for instance Theorem 5.1 p.58 in [33], there exists a subsequence of $(v^{(k)}, u_e^{(k)}, \mathbf{w}^{(k)}, \mathbf{z}^{(k)}, \bar{\boldsymbol{\varrho}}^{(k)})$, denoted by the same indices, such that

$$(3.21) \qquad \begin{aligned} & v^{(k)} \rightharpoonup v \text{ in } L^2(0,T;H^1(\Omega)), \quad \text{and} \quad \frac{d}{dt}v^{(k)} \rightharpoonup \frac{d}{dt}v \text{ in } L^2(0,T;(H^1(\Omega))^*), \\ & u_e^{(k)} \rightharpoonup u_e \text{ in } L^2(0,T;H^1(\Omega)), \\ & \mathbf{w}^{(k)} \rightharpoonup \mathbf{w} \text{ in } L^2(0,T;L^2(\Omega))^k, \quad \text{and} \quad \frac{\partial}{\partial t}\mathbf{w}^{(k)} \rightharpoonup \frac{\partial}{\partial t}\mathbf{w} \text{ in } L^2(Q)^k, \\ & \mathbf{z}^{(k)} \rightharpoonup \mathbf{z} \text{ in } L^2(0,T;L^2(\Omega))^m, \quad \text{and} \quad \frac{\partial}{\partial t}\mathbf{z}^{(k)} \rightharpoonup \frac{\partial}{\partial t}\mathbf{z} \text{ in } L^2(Q)^m. \end{aligned}$$

By the Rellich-Kondrachov compactness theorem (see [23], p. 286), since $v^{(k)}, u_e^{(k)}$ are bounded in $L^2(0,T;H^1(\Omega))$, we can assume that $v^{(k)} \to v$ and $u_e^{(k)} \to u_e$ strong in $L^2(Q)$.

Since $v^{(k)}, w_j^{(k)}$, for $j = 1, \ldots, k$, and $z_i^{(k)}$ for $i = 1, \ldots, m$, are weakly convergent and $\psi\phi'(t) \in L^2(Q) \cap L^2(0,T;H^1(\Omega))$, for any fixed $\phi \in \mathcal{D}(0,T)$ and $\psi \in \mathcal{C}_0^\infty(\mathbb{R}^d)$, we naturally have

$$(3.22) \qquad -\int_0^T \int_\Omega \frac{d}{dt}v^{(k)}(t)\psi\phi \, dxt = \int_0^T \int_\Omega v^{(k)}(t)\psi\phi'(t) \, dxt \xrightarrow[k\to+\infty]{} \int_0^T \int_\Omega v(t)\psi\phi'(t) \, dxt,$$

$$(3.23) \qquad -\int_0^T \int_\Omega \frac{d}{dt}w_j^{(k)}(t)\psi\phi \, dxt = \int_0^T \int_\Omega w_j^{(k)}(t)\psi\phi'(t) \, dxt \xrightarrow[k\to+\infty]{} \int_0^T \int_\Omega w_j(t)\psi\phi'(t) \, dxt,$$

$$(3.24) \qquad -\int_0^T \int_\Omega \frac{d}{dt} z_i^{(k)}(t)\psi\phi dxt = \int_0^T \int_\Omega z_i^{(k)}(t)\psi\phi'(t)dxt \xrightarrow[k\to+\infty]{} \int_0^T \int_\Omega z_i(t)\psi\phi'(t)dxt.$$

Let the corresponding bilinear and continuous forms on $H^1(\Omega) \times H^1(\Omega)$ associated with $\boldsymbol{\sigma}_{i,e}$ be $a_{i,e}$ as follows:

$$(3.25) \qquad a_{i,e}(u,\varphi) = \int_\Omega \boldsymbol{\sigma}_{i,e}\nabla u.\nabla\varphi dx,$$

and $\psi\phi \in L^2(Q) \cap L^2(0,T;H^1(\Omega))$, for any fixed $\phi \in \mathcal{D}(0,T)$ and $\psi \in \mathcal{C}_0^\infty(\mathbb{R}^d)$, we have

$$(3.26) \qquad \int_0^T a_{i,e}(u^{(k)}(t),\phi(t)\psi)dt \xrightarrow[k\to+\infty]{} \int_0^T a_{i,e}(u(t),\phi(t)\psi)dt.$$

Concerning the non-linear terms in (4.1), we use the equations (2.2)-(2.4)-(2.6) and Assumptions 2.1 to write: For $j = 1,\ldots,k$,
$$(3.27)$$
$$\begin{aligned} F_j(v^{(k)},w_j^{(k)}) &= \alpha_j(v^{(k)})\big(1-w_j^{(k)}\big) - \beta_j(v^{(k)})w_j^{(k)}, \\ &= \alpha_j(v^{(k)}) - \big(\alpha_j(v^{(k)}) - \alpha_j(v)\big)w_j^{(k)} - \big(\beta_j(v^{(k)}) - \beta_j(v)\big)w_j^{(k)} - \big(\alpha_j(v) + \beta_j(v)\big)w_j^{(k)}. \end{aligned}$$

For $i = 1,\ldots,m$,

$$(3.28) \qquad \begin{aligned} G_i(\bar{\boldsymbol{\varrho}}^{(k)},v^{(k)},\mathbf{w}^{(k)},\mathbf{z}^{(k)}) &= \big(G_i(\bar{\boldsymbol{\varrho}}^{(k)},v^{(k)},\mathbf{w}^{(k)},\mathbf{z}^{(k)}) - G_i(\bar{\boldsymbol{\varrho}}^*,v^{(k)},\mathbf{w}^{(k)},\mathbf{z}^{(k)})\big) \\ &\quad + \big(G_i(\bar{\boldsymbol{\varrho}}^*,v^{(k)},\mathbf{w}^{(k)},\mathbf{z}^{(k)}) - G_i(\bar{\boldsymbol{\varrho}}^*,v,\mathbf{w},\mathbf{z})\big) \\ &\quad + G_i(\bar{\boldsymbol{\varrho}}^*,v,\mathbf{w},\mathbf{z}). \end{aligned}$$

and

$$(3.29) \qquad I_{ion}(\bar{\boldsymbol{\varrho}}^{(k)},v^{(k)},\mathbf{w}^{(k)},\mathbf{z}^{(k)}) = \sum_{i=1}^N \bar{\varrho}_i^{(k)} y_i(v^{(k)}) \prod_{j=1}^k w_j^{p_{j,i},(k)}\big(v^{(k)} - C + \bar{\gamma}_i \log(z_i^{(k)})\big).$$

Starting by (3.27), we have $v^{(k)} \to v$ a.e in Q and α_j is continuous (of class $\mathcal{C}^\infty$), so that $\alpha_j(v^{(k)}) \to \alpha_j(v)$ a.e in Q, and $\alpha_j(v^{(k)})$ is bounded in $L^2(Q)$. It follows from a classical result, see Lemma 1.3 in [33], that $\alpha_j(v^{(k)}) \rightharpoonup \alpha_j(v)$ weak in $L^2(Q)$:

$$(3.30) \qquad \forall\phi \in \mathcal{D}(0,T), \quad \int_0^T < \alpha_j(v^{(k)}(t)),\phi(t)\psi > dt \xrightarrow[k\to+\infty]{} \int_0^T < \alpha_j(v(t)),\phi(t)\psi > dt.$$

As $\big(\alpha_j(v) + \beta_j(v)\big)\phi(t)\psi \in L^2(Q)$, the weak convergence of $w_j^{(k)}$ in $L^2(Q)$ implies that:
$$(3.31)$$
$$\forall\phi \in \mathcal{D}(0,T), \quad \int_0^T < \big(\alpha_j(v)+\beta_j(v)\big)w_j^{(k)}(t),\phi(t)\psi > dt \xrightarrow[k\to+\infty]{} \int_0^T < \big(\alpha_j(v)+\beta_j(v)\big)w_j(t),\phi(t)\psi > dt.$$

The remaining term in α_j is such that

$$(3.32) \qquad \left|\int_0^T \int_\Omega \big(\alpha_j(v^{(k)}) - \alpha_j(v)\big)w_j^{(k)}(t)\phi(t)\psi dxdt\right| \leqslant \|\big(\alpha_j(v^{(k)}) - \alpha_j(v)\big)\phi(t)\psi\|_{L^2(Q)}\|w_j^{(k)}\|_{L^2(Q)},$$

and similarly for β_j,

$$(3.33) \qquad \left|\int_0^T \int_\Omega \big(\beta_j(v^{(k)}) - \beta_j(v)\big)w_j^{(k)}(t)\phi(t)\psi dxdt\right| \leqslant \|\big(\beta_j(v^{(k)}) - \beta_j(v)\big)\phi(t)\psi\|_{L^2(Q)}\|w_j^{(k)}\|_{L^2(Q)}.$$

Since $v^{(k)} \to v$ a.e in Q and α_j, β_j are continuous (of class $\mathcal{C}^\infty$), we have

(3.34)
$$\forall \phi \in \mathcal{D}(0,T), \quad \|(\alpha_j(v^{(k)}) - \alpha_j(v))\phi(t)\psi\|_{L^2(Q)} \xrightarrow[k\to+\infty]{} 0,$$
$$\|(\beta_j(v^{(k)}) - \beta_j(v))\phi(t)\psi\|_{L^2(Q)} \xrightarrow[k\to+\infty]{} 0.$$

Since $\|w_j^{(k)}\|_{L^2(Q)}$ is bounded, we finally have

(3.35)
$$\forall \phi \in \mathcal{D}(0,T), \quad \int_0^T < (\alpha_j(v^{(k)}) - \alpha_j(v))w_j^{(k)}(t), \phi(t)\psi > dt \xrightarrow[k\to+\infty]{} 0,$$

(3.36)
$$\forall \phi \in \mathcal{D}(0,T), \quad \int_0^T < (\beta_j(v^{(k)}) - \beta_j(v))w_j^{(k)}(t), \phi(t)\psi > dt \xrightarrow[k\to+\infty]{} 0.$$

Let the non-linear term (3.28) associated with $\{\bar{\boldsymbol{\varrho}}^{(k)}, \bar{\boldsymbol{\varrho}}^*\}$ be $\{\bar{\mathcal{G}}^k, \bar{\mathcal{G}}^*\}$, for $i = 1, \ldots, m$:

(3.37)
$$\bar{\mathcal{G}}^k = < G_i(\bar{\boldsymbol{\varrho}}^{(k)}, v, \mathbf{w}, \mathbf{z}), \varphi >, \quad \text{and} \quad \bar{\mathcal{G}}^* = < G_i(\bar{\boldsymbol{\varrho}}^*, v, \mathbf{w}, \mathbf{z}), \varphi > .$$

We have $v^{(k)} \to v$, $\mathbf{w}^{(k)} \to \mathbf{w}$ and $\mathbf{z}^{(k)} \to \mathbf{z}$ a.e in Q, and G_i is a Lipschitz-continuous function, then for any fixed $\phi \in \mathcal{D}(0,T)$ and $\psi \in \mathcal{C}_0^\infty(\mathbb{R}^d)$, we have

(3.38)
$$\int_0^T < (G_i(\bar{\boldsymbol{\varrho}}^*, v^{(k)}(t), \mathbf{w}^{(k)}(t), \mathbf{z}^{(k)}(t)) - G_i(\bar{\boldsymbol{\varrho}}^*, v(t), \mathbf{w}(t), \mathbf{z}(t))), \phi(t)\psi > dt \xrightarrow[k\to+\infty]{} 0.$$

In the same way, since $\bar{\boldsymbol{\varrho}}^{(k)} \rightharpoonup \bar{\boldsymbol{\varrho}}^*$ weak in $L^\infty(\Omega)^N$ and G_i is a Lipschitz-continuous function, for any fixed $\phi \in \mathcal{D}(0,T)$ and $\psi \in \mathcal{C}_0^\infty(\mathbb{R}^d)$, we have
(3.39)
$$\int_0^T < (G_i(\bar{\boldsymbol{\varrho}}^{(k)}, v^{(k)}(t), \mathbf{w}^{(k)}(t), \mathbf{z}^{(k)}(t)) - G_i(\bar{\boldsymbol{\varrho}}^*, v^{(k)}(t), \mathbf{w}^{(k)}(t), \mathbf{z}^{(k)}(t))), \phi(t)\psi > dt \xrightarrow[k\to+\infty]{} 0.$$

Similary, for the non-linear ionic term (3.29), Let

(3.40)
$$\begin{aligned} I_{ion}(\bar{\boldsymbol{\varrho}}^{(k)}, v^{(k)}, \mathbf{w}^{(k)}, \mathbf{z}^{(k)}) &= I_{ion}(\bar{\boldsymbol{\varrho}}^{(k)}, v^{(k)}, \mathbf{w}^{(k)}, \mathbf{z}^{(k)}) - I_{ion}(\bar{\boldsymbol{\varrho}}^*, v^{(k)}, \mathbf{w}^{(k)}, \mathbf{z}^{(k)}) \\ &\quad + I_{ion}(\bar{\boldsymbol{\varrho}}^*, v^{(k)}, \mathbf{w}^{(k)}, \mathbf{z}^{(k)}) - I_{ion}(\bar{\boldsymbol{\varrho}}^*, v, \mathbf{w}, \mathbf{z}) \\ &\quad + I_{ion}(\bar{\boldsymbol{\varrho}}^*, v, \mathbf{w}, \mathbf{z}). \end{aligned}$$

Since $\bar{\boldsymbol{\varrho}}^{(k)} \rightharpoonup \bar{\boldsymbol{\varrho}}^*$ weak in $L^\infty(\Omega)^N$, $v^{(k)} \to v$, $\mathbf{w}^{(k)} \to \mathbf{w}$ and $\mathbf{z}^{(k)} \to \mathbf{z}$ a.e in Q, and I_{ion} is a bounded continuous function in $L^2(Q)$, we have
(3.41)
$$\int_0^T < (I_{ion}(\bar{\boldsymbol{\varrho}}^*, v^{(k)}, \mathbf{w}^{(k)}, \mathbf{z}^{(k)}) - I_{ion}(\bar{\boldsymbol{\varrho}}^*, v, \mathbf{w}, \mathbf{z})), \phi(t)\psi > dt \xrightarrow[k\to+\infty]{} 0, \quad \forall \phi \in \mathcal{D}(0,T), \ \psi \in \mathcal{C}_0^\infty(\mathbb{R}^d).$$

Also, since I_{ion} is linear with respect to $\bar{\boldsymbol{\varrho}} := \{\bar{\varrho}_i\}_{1 \leqslant i \leqslant N}$, for any fixed $\phi \in \mathcal{D}(0,T)$ and $\psi \in \mathcal{C}_0^\infty(\mathbb{R}^d)$, we have
(3.42)
$$\int_0^T < (I_{ion}(\bar{\boldsymbol{\varrho}}^{(k)}, v^{(k)}, \mathbf{w}^{(k)}, \mathbf{z}^{(k)}) - I_{ion}(\bar{\boldsymbol{\varrho}}^*, v^{(k)}, \mathbf{w}^{(k)}, \mathbf{z}^{(k)})), \phi(t)\psi > dt$$
$$= \int_0^T < \left(\sum_{i=1}^N (\varrho_i^{(k)} - \bar{\varrho}_i^*) y_i(v^{(k)}) \prod_{j=1}^k w_j^{p_{j,i},(k)} (v^{(k)} - C + \bar{\gamma}_i \log(z_i^{(k)})) \right), \phi(t)\psi > dt \xrightarrow[k\to+\infty]{} 0$$

Since Ω has Lipschitz boundary, it then satisfies the segment condition (see [3], p.68, definition. 3.21), We say $\mathcal{C}_0^\infty(\mathbb{R}^d)$ is dense in $H^1(\Omega)$, (see [3] theorem. 3.22). Therefore from (3.42), we have
(3.43)
$$\int_0^T < \left(I_{ion}(\bar{\boldsymbol{\varrho}}^{(k)}, v^{(k)}, \mathbf{w}^{(k)}, \mathbf{z}^{(k)}) - I_{ion}(\bar{\boldsymbol{\varrho}}^*, v^{(k)}, \mathbf{w}^{(k)}, \mathbf{z}^{(k)}) \right), \phi(t)\varphi > dt \underset{k \to +\infty}{\longrightarrow} 0, \quad \forall \phi \in \mathcal{D}(0,T), \ \varphi \in H^1(\Omega).$$

Combined (3.43) with limit (3.41), it implies
(3.44)
$$\int_0^T < \left(I_{ion}(\bar{\boldsymbol{\varrho}}^{(k)}, v^{(k)}, \mathbf{w}^{(k)}, \mathbf{z}^{(k)}) - I_{ion}(\bar{\boldsymbol{\varrho}}^*, v, \mathbf{w}, \mathbf{z}) \right), \phi(t)\varphi > dt \underset{k \to +\infty}{\longrightarrow} 0, \quad \forall \phi \in \mathcal{D}(0,T), \ \varphi \in H^1(\Omega).$$

Similarly, from (3.39)-(3.38), we can show
(3.45)
$$\int_0^T < \left(G_i(\bar{\boldsymbol{\varrho}}^{(k)}, v^{(k)}, \mathbf{w}^{(k)}, \mathbf{z}^{(k)}) - G_i(\bar{\boldsymbol{\varrho}}^*, v, \mathbf{w}, \mathbf{z}) \right), \phi(t)\varphi > dt \underset{k \to +\infty}{\longrightarrow} 0, \quad \forall \phi \in \mathcal{D}(0,T), \ \varphi \in H^1(\Omega).$$

By passing to the limit in the equations satisfied by $(v^{(k)}, u_e^{(k)}, \mathbf{w}^{(k)}, \mathbf{z}^{(k)}, \bar{\boldsymbol{\varrho}}^{(k)})$, we obtain that $(v, u_e, \mathbf{w}, \mathbf{z}, \bar{\boldsymbol{\varrho}}^*)$ is a solution to the bidomain system (2.1).

We conclude that $\bar{\varrho}^*$ realizes the minimum of $\mathcal{J}$. In fact, from the weak-* convergence (3.20), it follows that $\bar{\boldsymbol{\varrho}}^{(k)}$ is also weakly convergent in $L^2(\Omega)^N$.

By the weak lower semi-continuity of the regularisation term $\int_\Omega |\bar{\boldsymbol{\varrho}}^*|^2 \, dx$ in $L^2(\Omega)^N$, we deduce that

(3.46)
$$\begin{aligned} \mathcal{J}(v, \bar{\boldsymbol{\varrho}}^*) &\leqslant \lim_{k \to +\infty} \inf \mathcal{J}(v^{(k)}, \bar{\boldsymbol{\varrho}}^{(k)}), \\ &= \inf_{\bar{\boldsymbol{\varrho}} \in \mathcal{C}_{ad}} \mathcal{J}(v, \bar{\boldsymbol{\varrho}}), \end{aligned}$$

and the existence of a minimizer is proved.   ∎

Now, we demonstrate the numerical procedure to solve the optimality system (3.1).

4. NUMERICAL APPROXIMATION

In this section, we give a brief overview of the space and time discretization techniques to solve the primal (2.1) and adjoint (3.10) equations numerically. We use a finite element method (FEM) for the spatial discretization and a semi-implicit Euler scheme for the temporal discretization. We solve the optimal control problem (3.1) using the gradient descent method.

4.1. **Space and time Discretization of the bidomain model.** Here we give a description of the spatial discretization of the primal problem by a finite element method based on the weak formulation. A weak

solution triple $(v, \mathbf{w}, \mathbf{z})$ satisfies:

(4.1)

- $\int_\Omega A_m\big(C_m\partial_t v + I_{ion}(\bar{\boldsymbol{\varrho}}, v, \mathbf{w}, \mathbf{z}) - I_{app}\big)\psi dx + \int_\Omega \boldsymbol{\sigma}_i(\nabla v + \nabla u_e).\nabla\psi dx = 0,$

  $\forall\psi \in H^1(\Omega)$, for a.a. $t \in (0, T)$,

- $\int_\Omega \big(\boldsymbol{\sigma}_i\nabla v + (\boldsymbol{\sigma}_i + \boldsymbol{\sigma}_e)\nabla u_e\big).\nabla\psi dx = 0, \quad \forall\psi \in H^1(\Omega)$, with $\int_\Omega \psi dx = 0$, for a.a. $t \in (0, T)$,

- $\int_\Omega (\partial_t\mathbf{w} - \boldsymbol{F}(v, \mathbf{w})).\boldsymbol{\psi} dx = 0, \quad \forall\boldsymbol{\psi} \in L^2(\Omega)^k$, for a.a. $t \in (0, T)$,

- $\int_\Omega (\partial_t\mathbf{z} - \boldsymbol{G}(\bar{\boldsymbol{\varrho}}, v, \mathbf{w}, \mathbf{z})).\boldsymbol{\psi} dx = 0, \quad \forall\boldsymbol{\psi} \in L^2(\Omega)^m$, for a.a. $t \in (0, T)$,

  with $v(x, 0) = v_0(x)$, $\mathbf{w}(x, 0) = \mathbf{w}_0(x)$, and $\mathbf{z}(x, 0) = \mathbf{z}_0(x)$, for almost all $x \in \Omega$.

Let $\mathcal{V}^h \subset H^1(\Omega)$ be the finite dimensional subspace of piecewise linear basis functions with respect to the spatial grid for the approximation of electrical potentials, gating variables and concentration variables. The approximate solutions of the vectors $\boldsymbol{V} \in \mathbb{R}^M$ and $\boldsymbol{U} \in \mathbb{R}^M$ and matrices $\boldsymbol{W} \in \mathbb{R}^{k\times M}$ and $\boldsymbol{Z} \in \mathbb{R}^{m\times M}$ are expressed in the form:

(4.2)
$$\boldsymbol{V}(t) = \sum_{i=1}^M v_i(t)\omega_i, \quad \boldsymbol{U}(t) = \sum_{i=1}^M u_e^i(t)\omega_i, \quad \boldsymbol{W}(t) = \big\{\boldsymbol{W}^{(j)}(t)\big\}_{j=1}^k = \big\{\sum_{i=1}^M w_i^{(j)}(t)\omega_i\big\}_{j=1}^k,$$
$$\boldsymbol{Z}(t) = \big\{\boldsymbol{Z}^{(j')}(t)\big\}_{j'=1}^m = \big\{\sum_{i=1}^M z_i^{(j')}(t)\omega_i\big\}_{j'=1}^m,$$

where $\{\omega_i\}_{i=1}^M$ denote the basis functions, and M is the number of nodal points at the tissue domain. We recall that the variables k and m correspond to the number of gating variables $\mathbf{w}$ and intracellular concentration variables $\mathbf{z} \in \mathbb{R}^m$, respectively, verifying the ODEs of the bidomain system (2.1).

The semi-discretization of the primal equations in space results in the differential algebraic system is given as follows:

(4.3) $$A_m C_m \boldsymbol{M}\frac{\partial}{\partial t}\boldsymbol{V} = -\boldsymbol{A_i}\boldsymbol{V} - \boldsymbol{A_i}\boldsymbol{U} + A_m\boldsymbol{M}\big(\mathcal{I_{app}} - \mathcal{I_{ion}}(\bar{\boldsymbol{\varrho}}, \boldsymbol{V}, \boldsymbol{W}^{(j)}, \boldsymbol{Z}^{(j')})\big),$$

(4.4) $$\boldsymbol{A_{ie}}\boldsymbol{U} = -\boldsymbol{A_i}\boldsymbol{V},$$

(4.5) $$\boldsymbol{M}\frac{\partial}{\partial t}\boldsymbol{W}^{(j)} = \mathcal{F}^{(j)}(\boldsymbol{V}, \boldsymbol{W}^{(j)}), \text{ for } j = 1, ..., k,$$

(4.6) $$\boldsymbol{M}\frac{\partial}{\partial t}\boldsymbol{Z}^{(j')} = \mathcal{G}^{(j')}(\bar{\boldsymbol{\varrho}}, \boldsymbol{V}, \boldsymbol{W}, \boldsymbol{Z}), \text{ for } j' = 1, ..., m,$$

along with initial conditions for $\boldsymbol{V}, \boldsymbol{W}^{(j)}$ and $\boldsymbol{Z}^{(j')}$, where $\boldsymbol{A_{ie}} = \{< (\boldsymbol{\sigma}_i + \boldsymbol{\sigma}_e)\nabla\omega_i, \nabla\omega_{j''} >\}_{i,j''=1}^M$ and $\boldsymbol{A_i} = \{< \boldsymbol{\sigma}_i\nabla\omega_i, \nabla\omega_{j''} >\}_{i,j''=1}^M$ are the stiffness matrices and $\boldsymbol{M} = \{< \omega_i, \omega_{j''} >\}_{i,j''=1}^M$ is the mass matrix. The vector $\mathcal{I_{app}}$ is defined by comuting at each component $\mathcal{I_{app}}_i(t) = I_{app}(x_i, t)$. The ith component of the vector $\mathcal{I_{ion}}(\bar{\boldsymbol{\varrho}}, \boldsymbol{V}, \boldsymbol{W}, \boldsymbol{Z})$ is equal to $I_{ion}\big(\bar{\boldsymbol{\varrho}}, v_i(t), \{w_i^{(j)}(t)\}_{j=1}^k, \{z_i^{(j')}(t)\}_{j'=1}^m\big)$

The resulting system is then discretized in time using a semi implicit scheme (Backward Euler formula). Let $\mathcal{N} \in \mathbb{N}$ be a given integer and consider a uniform partition $[t_n, t_{n+1}]$ for $0 \leqslant n \leqslant \mathcal{N}-1$, with $t_n = n\Delta t$, of the time interval of interest $[0, T]$, with a time step $\Delta t = T/\mathcal{N}$.

Denote by $(\mathbf{w}^n, \mathbf{z}^n, v^n, u_e^n)$ the approximated solution obtained at time t_n. Then $(\mathbf{w}^{n+1}, \mathbf{z}^{n+1}, v^{n+1}, u_e^{n+1})$ is computed as follows: For $0 \leqslant n \leqslant \mathcal{N} - 1$

　　1. Solve the ionic model, computing $\mathbf{w}^{n+1}, \mathbf{z}^{n+1}$ in each node of Ω.

Using the EDO formulation (2.4), we get an explicit numerical solution for each time step, being able to recover variables w_j, for $j = 1, \ldots, k$, as

(4.7)
$$\begin{cases} w_j^{n+1} = e^{-(\alpha_j^n + \beta_j^n)\Delta t}\left(w_j^n - \dfrac{\alpha_j^n}{\alpha_j^n + \beta_j^n}\right) + \dfrac{\alpha_j^n}{\alpha_j^n + \beta_j^n}, \quad n = 0, \ldots, \mathfrak{n}, \\ \\ w_j(0) = w_{j,0}. \end{cases}$$

The explicit formula is employed for all the gating variables $\mathbf{w}$ of the ionic model (which are the majority of the unknowns of the ionic model). Therefore for the intracellular concentrations $\mathbf{z}$, we apply the backward Euler method: for $i = 1, \ldots, m$,

(4.8)
$$\frac{z_i^{n+1} - z_i^n}{\Delta t} = G_i(\bar{\varrho}, v^n, \mathbf{w}^{n+1}, \mathbf{z}^{n+1}), \quad \text{in } \Omega.$$

2. Evaluate in each node the ionic current $I_{ion}(\bar{\varrho}, v^n, \mathbf{w}^{n+1}, \mathbf{z}^{n+1})$.
3. With the computed ionic current, solve the first equation of the bidomain model (2.1) to compute the transmembrane potential $v^{n+1} \in \mathcal{V}^h$ using a first order semi-implicit scheme:

(4.9)
$$\int_\Omega A_m C_m \frac{v^{n+1} - v^n}{\Delta t}\phi dx + \int_\Omega \boldsymbol{\sigma}_i \nabla v^{n+1}.\nabla\phi dx = \int_\Omega A_m\left(I_{app}^{n+1} - I_{ion}(\bar{\varrho}, v^n, \mathbf{w}^{n+1}, \mathbf{z}^{n+1})\right)\phi dx - \int_\Omega \boldsymbol{\sigma}_i \nabla u_e^n.\nabla\phi dx.$$

4. With the computed transmembrane potential v^{n+1}, solve the second equation of the bidomain model (2.1) to compute the extracellular potential $u_e^{n+1} \in \mathcal{V}^h$:

(4.10)
$$\int_\Omega (\boldsymbol{\sigma}_i + \boldsymbol{\sigma}_e)\nabla u_e^{n+1}.\nabla\phi_e dx + \int_\Omega \boldsymbol{\sigma}_i \nabla v^{n+1}.\nabla\phi_e dx = 0.$$

Therefore, the equations (4.3) and (4.4) become the following matrix representation:

(4.11)
$$\begin{aligned} (\frac{A_m C_m}{\Delta t}\boldsymbol{M} + \boldsymbol{A_i})\boldsymbol{V}^{n+1} &= \frac{A_m C_m}{\Delta t}\boldsymbol{M}\boldsymbol{V}^n + A_m \boldsymbol{M}\left(\boldsymbol{\mathcal{I}_{app}}^{n+1} - \boldsymbol{\mathcal{I}_{ion}}(\bar{\varrho}, \boldsymbol{V}^n, \boldsymbol{W}^{n+1}, \boldsymbol{Z}^{n+1})\right) - \boldsymbol{A_i}\boldsymbol{U}^n, \\ \boldsymbol{A_{ie}}\boldsymbol{U}^{n+1} &= -\boldsymbol{A_i}\boldsymbol{V}^{n+1}. \end{aligned}$$

4.2. **Space and time Discretization of the adjoint problem.** We use an analogous numerical algorithm as for the primal problem (2.1) to discretize the dual equations (3.10) in the tissue domain. The approximate solutions $\boldsymbol{P}, \boldsymbol{Q}, \boldsymbol{R}$ and $\boldsymbol{S}$ can be expressed in the form:

(4.12)
$$\boldsymbol{P}(t) = \sum_{i=1}^M p_i(t)\omega_i, \quad \boldsymbol{Q}(t) = \sum_{i=1}^M q^i(t)\omega_i, \quad \boldsymbol{R}(t) = \{\boldsymbol{R}^{(j)}(t)\}_{j=1}^k = \{\sum_{i=1}^M r_i^{(j)}(t)\omega_i\}_{j=1}^k,$$
$$\boldsymbol{S}(t) = \{\boldsymbol{S}^{(j')}(t)\}_{j'=1}^m = \{\sum_{i=1}^M s_i^{(j')}(t)\omega_i\}_{j'=1}^m.$$

The following semi-discrete form of the dual problem is obtained:

(4.13)
$$\begin{aligned} -A_m C_m \boldsymbol{M}\frac{\partial}{\partial t}\boldsymbol{P} + A_m \boldsymbol{M}(\partial_{\boldsymbol{V}}\boldsymbol{\mathcal{I}_{ion}})^T\boldsymbol{P} &= -\boldsymbol{A_i}\boldsymbol{P} - \boldsymbol{A_i}\boldsymbol{Q} + \boldsymbol{M}(\partial_{\boldsymbol{V}}\boldsymbol{\mathcal{F}})^T\boldsymbol{R} + \boldsymbol{M}(\partial_{\boldsymbol{V}}\boldsymbol{\mathcal{G}})^T\boldsymbol{S} \\ &\quad + \epsilon_1 \boldsymbol{M}(\boldsymbol{V} - \boldsymbol{V}_{meas}), \\ \boldsymbol{A_{ie}}\boldsymbol{P} &= -\boldsymbol{A_i}\boldsymbol{Q}, \\ -\frac{\partial}{\partial t}\boldsymbol{R} + A_m(\partial_{\boldsymbol{W}}\boldsymbol{\mathcal{I}_{ion}})^T\boldsymbol{P} &= (\partial_{\boldsymbol{W}}\boldsymbol{\mathcal{F}})^T\boldsymbol{R} + (\partial_{\boldsymbol{Z}}\boldsymbol{\mathcal{G}})^T\boldsymbol{S}, \\ -\frac{\partial}{\partial t}\boldsymbol{S} + A_m(\partial_{\boldsymbol{Z}}\boldsymbol{\mathcal{I}_{ion}})^T\boldsymbol{P} &= (\partial_{\boldsymbol{Z}}\boldsymbol{\mathcal{G}})^T\boldsymbol{S}, \end{aligned}$$

with terminal conditions $\boldsymbol{P}(T) = \boldsymbol{R}^{(j)}(T) = \boldsymbol{S}^{(j')}(T) = \boldsymbol{0}, \forall j = 1, \ldots, k, \forall j' = 1, \ldots, m$. The derivative expression terms are defined as follows

(4.14)
$$\partial_{\boldsymbol{V}}\mathcal{I}_{ion}(\bar{\varrho}, \boldsymbol{V}, \boldsymbol{W}, \boldsymbol{Z}) := \big\{ \frac{\partial}{\partial v_i} I_{ion}\big(\bar{\varrho}, v_i(t), \{w_i^{(j)}(t)\}_{j=1}^k, \{z_i^{(j')}(t)\}_{j'=1}^m\big)\big\}_{i=1}^M \in \mathbb{R}^M,$$
$$\partial_{\boldsymbol{W}}\mathcal{I}_{ion}(\bar{\varrho}, \boldsymbol{V}, \boldsymbol{W}, \boldsymbol{Z}) := \big\{ \frac{\partial}{\partial w} I_{ion}\big(\bar{\varrho}, v_i(t), \{w_i^{(j)}(t)\}_{j=1}^k, \{z_i^{(j')}(t)\}_{j'=1}^m\big)\big\}_{i=1}^M \in \mathbb{R}^{k \times M},$$
$$\partial_{\boldsymbol{Z}}\mathcal{I}_{ion}(\bar{\varrho}, \boldsymbol{V}, \boldsymbol{W}, \boldsymbol{Z}) := \big\{ \frac{\partial}{\partial z} I_{ion}\big(\bar{\varrho}, v_i(t), \{w_i^{(j)}(t)\}_{j=1}^k, \{z_i^{(j')}(t)\}_{j'=1}^m\big)\big\}_{i=1}^M \in \mathbb{R}^{m \times M},$$
$$\partial_{\boldsymbol{V}}\mathcal{F}(\boldsymbol{V}, \boldsymbol{W}) := \big\{ \frac{\partial}{\partial v} F\big(v_i(t), \{w_i^{(j)}(t)\}_{j=1}^k\big)\big\}_{i=1}^M \in \mathbb{R}^{k \times M},$$
$$\partial_{\boldsymbol{W}}\mathcal{F}(\boldsymbol{V}, \boldsymbol{W}) := \big\{ \frac{\partial}{\partial w} F\big(v_i(t), \{w_i^{(j)}(t)\}_{j=1}^k\big)\big\}_{i=1}^M \in \mathbb{R}^{k \times k \times M},$$
$$\partial_{\boldsymbol{V}}\mathcal{G}(\bar{\varrho}, \boldsymbol{V}, \boldsymbol{W}, \boldsymbol{Z}) := \big\{ \frac{\partial}{\partial v} G\big(\bar{\varrho}, v_i(t), \{w_i^{(j)}(t)\}_{j=1}^k, \{z_i^{(j')}\}_{j'=1}^m\big)\big\}_{i=1}^M \in \mathbb{R}^{m \times M}.$$
$$\partial_{\boldsymbol{W}}\mathcal{G}(\bar{\varrho}, \boldsymbol{V}, \boldsymbol{W}, \boldsymbol{Z}) := \big\{ \frac{\partial}{\partial w} G\big(\bar{\varrho}, v_i(t), \{w_i^{(j)}(t)\}_{j=1}^k, \{z_i^{(j')}\}_{j'=1}^m\big)\big\}_{i=1}^M \in \mathbb{R}^{k \times m \times M}.$$
$$\partial_{\boldsymbol{Z}}\mathcal{G}(\bar{\varrho}, \boldsymbol{V}, \boldsymbol{W}, \boldsymbol{Z}) := \big\{ \frac{\partial}{\partial z} G\big(\bar{\varrho}, v_i(t), \{w_i^{(j)}(t)\}_{j=1}^k, \{z_i^{(j')}\}_{j'=1}^m\big)\big\}_{i=1}^M \in \mathbb{R}^{m \times m \times M}.$$

For $i = 1, \ldots M$, let's denote by $\boldsymbol{R}_i^n = \{R_i^{(j),n}\}_{j=1}^k \in \mathbb{R}^k$, the value of the adjoint state with respect to $\boldsymbol{w}$ and $\boldsymbol{Z}_i^n = \{Z_i^{(j'),n}\}_{j'=1}^m \in \mathbb{R}^m$, the value of the adjoint state with respect to $\boldsymbol{z}$ at the node x_i and at time t^n, the computation of these two variables is performed point-wise as follows.

Step 1: For i=1,…, M, solve
(4.15)
$$\begin{cases} \big(\frac{1}{\Delta t}\boldsymbol{I} - ((\partial_{\boldsymbol{W}}\mathcal{F})_i^n)^T\big)\boldsymbol{R}_i^n &= \frac{1}{\Delta t}\boldsymbol{R}_i^{n+1} - A_m\big((\partial_{\boldsymbol{W}}\mathcal{I}_{ion})_i^{n+1}\big)^T \boldsymbol{P}_i^{n+1} + \big((\partial_{\boldsymbol{W}}\mathcal{G})_i^{n+1}\big)^T \boldsymbol{S}_i^{n+1}, \\ \big(\frac{1}{\Delta t}\boldsymbol{I} - ((\partial_{\boldsymbol{Z}}\mathcal{G})_i^n)^T\big)\boldsymbol{S}_i^n &= \frac{1}{\Delta t}\boldsymbol{S}_i^{n+1} - A_m((\partial_{\boldsymbol{Z}}\mathcal{I}_{ion})_i^{n+1})^T \boldsymbol{P}_i^{n+1}. \end{cases}$$

Step 2:
(4.16)
$$\begin{cases} \big(\frac{A_m C_m}{\Delta t}\boldsymbol{M} + \boldsymbol{A_i}\big)\boldsymbol{P}^n &= A_m \boldsymbol{M}\big[\big(\frac{C_m}{\Delta t}\mathbb{1} - (\partial_{\boldsymbol{V}}\mathcal{I}_{ion})^{n+1}\big) * \boldsymbol{P}^{n+1}\big] + \epsilon_1 \boldsymbol{M}(\boldsymbol{V}^n - \boldsymbol{V}_{meas}^n) \\ &\quad + \boldsymbol{M} \sum_{j'=1}^m (\partial_{\boldsymbol{V}}\mathcal{G}^{(j'),n}) * \boldsymbol{S}^{(j'),n} - \boldsymbol{A_i}\boldsymbol{Q}^{n+1} + \boldsymbol{M} \sum_{j=1}^k (\partial_{\boldsymbol{V}}\mathcal{F}^{(j)})^n * \boldsymbol{R}^{(j),n}, \\ \boldsymbol{A_{ie}}\boldsymbol{Q}^n &= -\boldsymbol{A_i}\boldsymbol{P}^n. \end{cases}$$

Here, $\mathbb{1} \in \mathbb{R}^M$ is a vector filled with the value 1 and the multiplication "*" is performed point-wise.

Remark 4.1. *The retrograde problem (3.10) is fully linear, we use a first order semi-implicit scheme to solve it. The reason is that we separate the ODE system variables $\boldsymbol{R}$ and $\boldsymbol{S}$ from the PDE variables $\boldsymbol{P}$ and $\boldsymbol{Q}$. We also solve the bidomain problem sequentially, we first compute $\boldsymbol{P}$ and then we compute $\boldsymbol{Q}$. This follows the same scheme developed for the primal problem in [24].*

4.3. **Optimization algorithm.** Given an initial guess of maximal conductance parameters $\bar{\varrho}_{guess}$, we solve the optimization problem using the following algorithm based on a gradient descent method.

Algorithm 1 Optimization of the maximal conductance parameters $\bar{\varrho}$

$\bar{\varrho} = \bar{\varrho}_{guess}$,
Solve state problem,
Solve adjoint problem,
while $\mathcal{I}(\bar{\varrho}) > \epsilon_{Func}$ & $\|\frac{\mathcal{DI}}{\mathcal{D}\bar{\varrho}}\| > \epsilon_{Grad}$ & $iter \leqslant MaxIterNumber$ **do**
$\quad \bar{\varrho} = \bar{\varrho} - \alpha \times \frac{\mathcal{DI}}{\mathcal{D}\bar{\varrho}}$.
$\quad$ Solve state problem,
$\quad$ Solve adjoint problem,
$\quad$ Compute the cost function and its gradient,
end while
$\bar{\varrho}_{optim} = \bar{\varrho}$.

Here, ϵ_{Func} and ϵ_{Grad} are positive constants defining the desired tolerance on the cost function and its gradient respectively. The coefficient α is positive and could be fixed or updated at each iteration and $MaxIterNumber$ stands for the maximal number of iterations in the optimization procedure.

5. NUMERICAL RESULTS

In this section, numerical results on the basis of two different test cases are presented. In all tests, the computational domain $\Omega = [0,1] \times [0,1] \subset \mathbb{R}^2$ of size 1 cm^2 is fixed and a triangular discretization is used which consists of 5718 elements and 2960 nodes. During the simulations, we fix the time step length $\Delta t = 0.1ms$. The termination of the optimization algorithm is based on the following condition: $\epsilon_{Func} = 10^{-8}$ and $\epsilon_{Grad} = 10^{-8}$. For all the following tests, the desired transmembrane potential v_{meas} is simulated with the physiological Luo Rudy phase I model with its original control parameters using a prescribed time course of a stimulation current which its magnitude is $I_{app}(t) = 80\mu A/cm^2$ and its duration is $1ms$.

5.1. **Single maximal conductance parameter estimation:**

In the first case, we consider to optimize separately three of the maximal conductance parameters $\bar{\varrho}_{Na}$, $\bar{\varrho}_{si}$, $\bar{\varrho}_{K1}$ representing three different ion channels: sodium, calcium and potassium, respectively. Moreover, if the stopp criteria conditions are not satisfied, the algorithm terminates within a prescribed number of iterations. Here the maximum number of iteration parameter $MaxIterNumber = 20$.

5.1.1. *Maximal conductance parameter of the fast inward sodium current $\bar{\varrho}_{Na}$:*

In this test, we present a numerical results of the estimation of the parameter $\bar{\varrho}_{Na}$. Since this parameter is mainly important in the depolarization phase, we consider the cost functional in the time window $[0ms, 20ms]$ of the simulation. The exact value $\overline{\varrho}_{Na}$ is equal to $23 \ mS/cm^2$. We generate the measurement v_{meas} by solving the forward problem using the exact value of $\overline{\varrho}_{Na}$ and we start our optimization procedure using a guess value $\overline{\varrho}_{Na,guess} = \frac{1}{2}\overline{\varrho}_{Na} = 11.5 \ mS/cm^2$. Since the cost function depends on the parameters ϵ_1 and ϵ_2 used to make a balance between the function of interest $\left(\int_Q |v(\overline{\varrho}_{Na}) - v_{meas}|^2 \, dxt\right)$ and the regularization term $\left(\int_\Omega |\overline{\varrho}_{Na}|^2 \, dx\right)$, we first run the optimization procedure with $\epsilon_1 = 1$ and we vary ϵ_2 from 0.05 to 0.001.
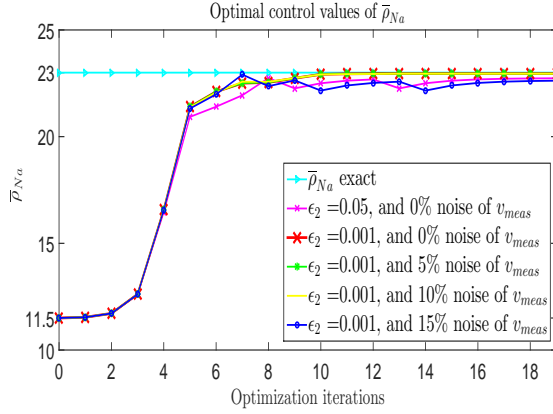
FIGURE 1. The optimal control solution for the optimization of $\bar{\varrho}_{Na}$ for different values of ϵ_2 and different levels of noise.

ϵ_2	Noise on v_{meas} (%)	$\dfrac{\left\| \overline{\varrho}_{Na,exact} - \overline{\varrho}_{Na} \right\|}{\left\| \overline{\varrho}_{Na,exact} \right\|} \times 10^2$
0.05	0 %	1.117 %
0.001	0 %	0.195 %
0.001	5 %	0.196 %
0.001	10 %	0.22 %
0.001	15 %	1.58 %

TABLE 1. Relative errors of the optimal control solution $\bar{\varrho}_{Na}$ for all cases.

As shown in Fig 1 for both cases, the optimization algorithm converges to the desired control value. But the accuracy is better with $\epsilon_2 = 0.001$ than $\epsilon_2 = 0.05$ as shown in Table1. From now, we fix $\epsilon_1 = 1$ and $\epsilon_2 = 0.001$.
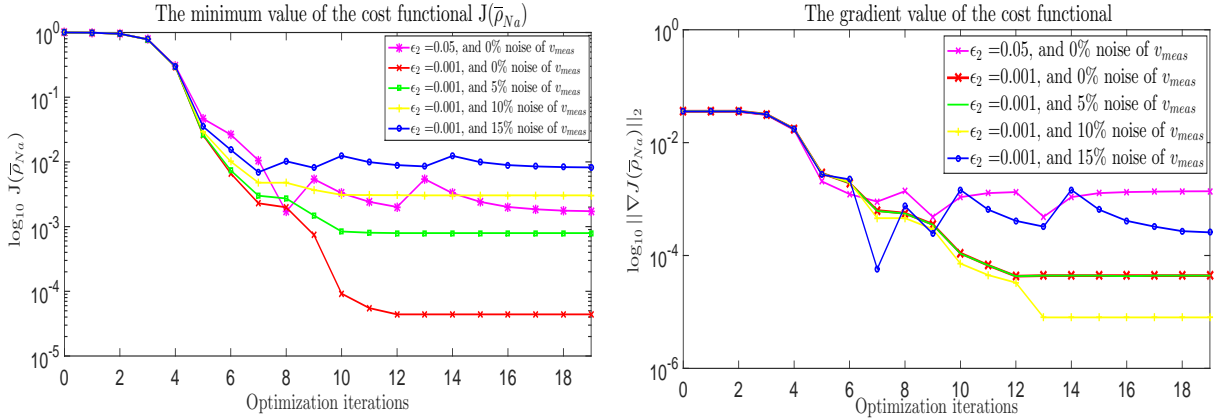
FIGURE 2. Left: Log scale plot of the cost function $\mathcal{I}(\bar{\varrho}_{Na})$. Right: Log scale plot of the norm of its gradient during the optimization procedure.

In order to test the robustness of the algorithm, we add different levels of gaussian noise to the measured data v_{meas}, and we solve the optimization problem following Algorithm 1 for each value of noise. As shown in Fig 1, the algorithm converges for all levels of noise. Table 1 shows that the accuracy is altered with the noise. But for 15% of noise, the relative error on the estimated value of $\bar{\varrho}_{Na}$ is under 2%. Figure 2 shows the evolution of the cost function $\mathcal{I}(\bar{\varrho}_{Na})$ and the norm of its gradient with respect to the optimization iterations for different regularization parameter values ϵ_2 and noise levels on the measured potential.

5.1.2. *Maximal conductance parameter of the slow inward-calcium related current $\bar{\varrho}_{si}$:*
 In this test, we present a numerical results for the optimization of the parameter $\bar{\varrho}_{si}$. Since this parameter acts on the plateau phase, we performed the optimization on a time window [0ms, 400ms]. We consider the

initial guess value $\bar{\varrho}_{si,guess} = \dfrac{3}{2}\bar{\varrho}_{si,exact} = 0.135\ mS/cm^2$. The Fig 3 shows the evolution of the parameter $\bar{\varrho}_{si}$ during the optimization procedure.
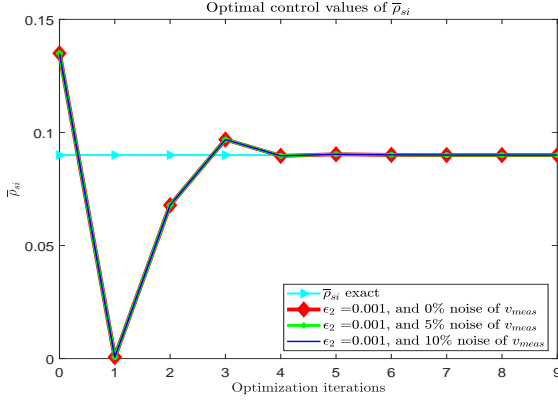

ϵ_2	Noise on v_{meas} (%)	$\dfrac{\|\bar{\varrho}_{si,exact} - \bar{\varrho}_{si}\|}{\|\bar{\varrho}_{si,exact}\|} \times 10^2$
0.001	0 %	3.26e-7 %
0.001	5 %	6.8e-4 %
0.001	10 %	2.37e-3 %

TABLE 2. Relative errors of the optimal control solution $\bar{\varrho}_{si}$ for all cases.

FIGURE 3. The optimal control solution for the optimization of $\bar{\varrho}_{si}$.

The table 2 shows the relative error of the obtained solution with respect to the 0%, 5% and 10% noise levels. We can see that it converge from the fourth iteration and the accuracy of the obtained optimal solution of $\bar{\varrho}_{si}$ seems to be less sensitive to noise compared to optimal solution of $\bar{\varrho}_{Na}$.
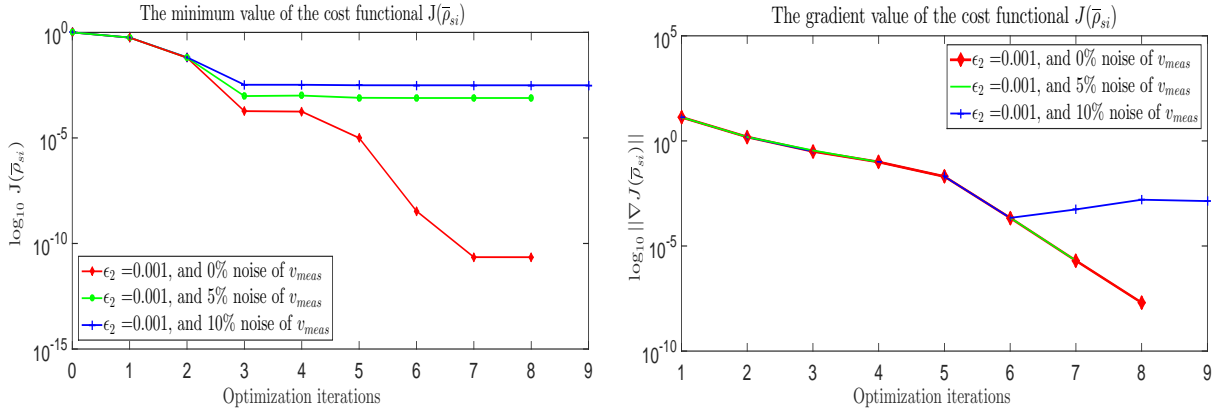
FIGURE 4. Left: Log scale plot of the cost function $\mathcal{I}(\bar{\varrho}_{si})$. Right: Log scale plot of the norm of its gradient during the optimization procedure.

5.1.3. *Maximal time-independent potassium maximal conductance parameter $\bar{\varrho}_{K1}$:*

In this test, we present a numerical results for the optimization of the parameter $\bar{\varrho}_{K1}$. Since this parameter acts on the repolarization phase, we performed the optimization on a time window [0ms, 400ms]. The initial guess considered is $\bar{\varrho}_{K1,guess} = \dfrac{3}{2}\bar{\varrho}_{K1,exact} = 0.90705\ mS/cm^2$. Fig 5 shows the evolution of the parameter $\bar{\varrho}_{K1}$ during the optimization procedure. The table 3 shows the relative error of the obtained solution with respect to the noise level.
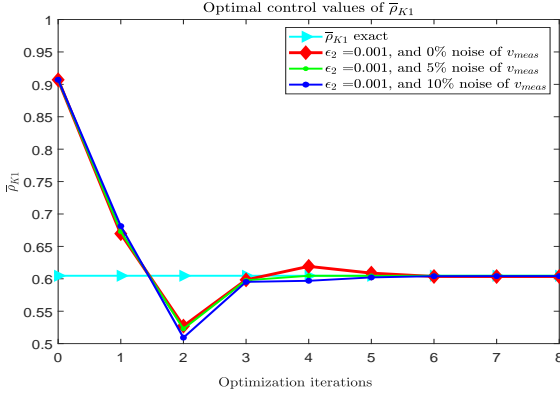
FIGURE 5. The evolution of the optimal control solution $\bar{\varrho}_{K1}$ during the optimization iterations.

ϵ_2	Noise on v_{meas} (%)	$\dfrac{\|\overline{\varrho}_{K1,exact} - \overline{\varrho}_{K1}\|}{\|\overline{\varrho}_{K1,exact}\|} \times 10^2$
0.001	0 %	0.0019 %
0.001	5 %	0.0042 %
0.001	10 %	0.083 %

TABLE 3. Relative errors of the optimal control solution $\bar{\varrho}_{K1}$ for different noise levels.

The results in the table 3 show that the optimal solution of $\bar{\varrho}_{K1}$ is more sensitive to the noise than $\bar{\varrho}_{si}$ and less sensitive to noise than $\bar{\varrho}_{Na}$.
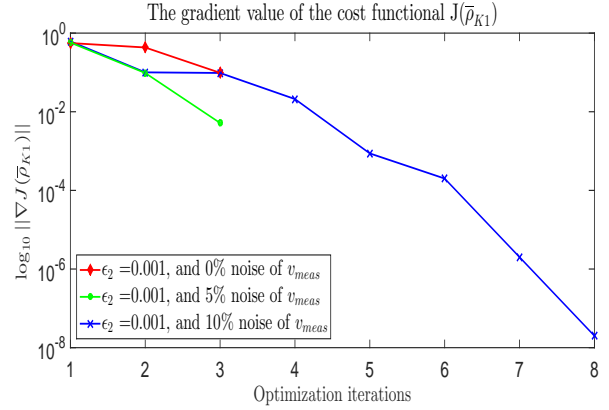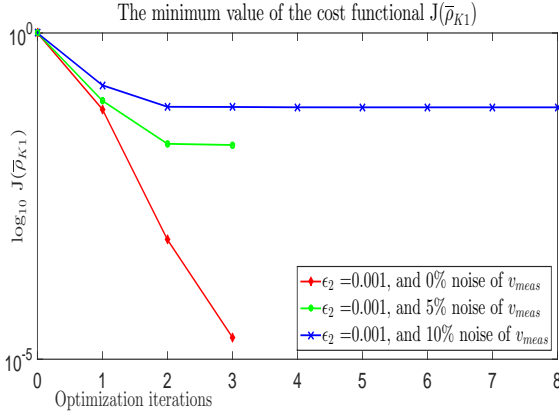

FIGURE 6. Left: Log scale plot of the cost function $\mathcal{I}(\bar{\varrho}_{K1})$. Right: Log scale plot of the norm of its gradient during the optimization procedure.

5.2. **Simultaneous estimate of the maximal conductances parameters:**
In this section, we aim to optimize all the maximal conductance parameters of LR1 model simultaneously. The parameters are: $\bar{\varrho}_{Na}$, $\bar{\varrho}_{si}$, $\bar{\varrho}_{K}$, $\bar{\varrho}_{K1}$, $\bar{\varrho}_{Kp}$ and $\bar{\varrho}_b$. The presented numerical results are based on fixing the regularisation parameters $\epsilon_1 = 1$, $\epsilon_2 = 0$, and adding different levels of gaussian noise to the measured data. First, we have to say that all our attempts to estimate multiple parameters from a single observation v_{meas} failed. Based on the theoretical work [2], the stability and the uniqueness of the parameter estimation inverse problem could be guaranteed using as much measurements as the number of the parameters to be optimized. In this work, we choose to modify the position of the stimuli in space in order to obtain the desired number of observations. Suppose that v^l_{meas} is the observation associated to the lth applied current

I_{app}^l, we look for the set of parameters $\bar{\boldsymbol{\varrho}} := \{\bar{\varrho}_i\}_{1 \leqslant i \leqslant N}$ that solves the following minimization problem:

(5.1) $(\mathcal{P})$ $\begin{cases} \min\limits_{\bar{\boldsymbol{\varrho}} \in \mathcal{C}_{ad}} \mathcal{I}(\bar{\boldsymbol{\varrho}}) = \dfrac{1}{2} \sum\limits_{l=1}^{N_S} \int_Q \left| v^l(\bar{\boldsymbol{\varrho}}) - v_{meas}^l \right|^2 dxt, \\[2mm] \text{subject to: } v^l \text{ is solution of the coupled PDE system (2.1) where } I_{app} = I_{app}^l. \end{cases}$

Here N_S is the number of stimulus currents with $N_S \geqslant N$. Without loss of generality, using the same strategy presented in paragraph 3.1, the computation of the cost function gradient for multiple observations is given by

(5.2) $$\frac{\mathcal{D}\mathcal{J}}{\mathcal{D}\bar{\boldsymbol{\varrho}}} = \sum_{l=1}^{N_S} \left(\int_Q (\frac{\partial \boldsymbol{G}}{\partial \bar{\boldsymbol{\varrho}}})^T \boldsymbol{s}^l dxdt - \int_Q A_m p^l \frac{\partial}{\partial \bar{\boldsymbol{\varrho}}} I_{ion} dxdt \right),$$

where $(p^l, q^l, \boldsymbol{r}^l, \boldsymbol{s}^l)$ is the adjoint state of $(v^l, u_e^l, \boldsymbol{w}^l, \boldsymbol{z}^l)$ solution of the system (2.1) where $I_{app} = I_{app}^l$.
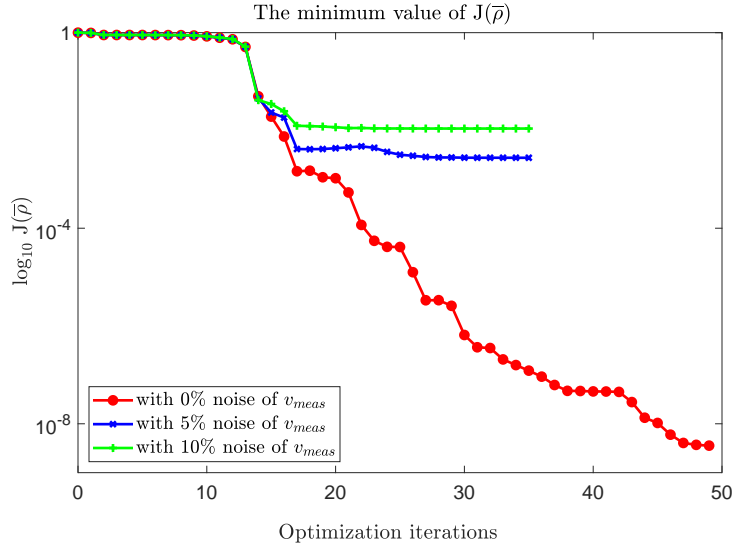

FIGURE 7. Log scale plot of the cost function $\mathcal{I}(\bar{\varrho})$ during the optimization procedure.

Figure 7 shows the evolution of the cost function with respect to the optimization iteration. We remark that in the noise free case (red line) the cost function achieves 10^{-8}, whereas for the noisy observation cases the cost function almost stagnates from iteration 30 achieving 2.76e-3 (respectively 1.09e-2) for 5% (respectively 10%) of noise level. Table 4 provides the error percentage of each of the estimated parameters with respect of the noise level. We remark that the accuracy of the estimated parameters is higher than 98% even for 5 and 10 % of noise level. We, particularly, notice that the error on the $\bar{\varrho}_{Na}$ parameter is less than 0.056% for the three cases which might reveal the sensitivity of the model with respect to the $\bar{\varrho}_{Na}$.

Noise levels (%)	$\bar{\varrho}_{Na}$	$\bar{\varrho}_{si}$	$\bar{\varrho}_{K}$	$\bar{\varrho}_{K1}$	$\bar{\varrho}_{Kb}$	$\bar{\varrho}_{b}$
0 %	0.0098 %	0.1967 %	1.0509 %	0.0764 %	0.0578 %	0.1181 %
5 %	0.0552 %	0.4470 %	1.9545 %	0.5021 %	0.3921 %	0.0043 %
10 %	0.0498 %	0.23 %	0.9467 %	0.3302 %	0.4888 %	0.0356 %

TABLE 4. Error percentage of the optimal control solution for the different noise levels on the measured potentials $(v_{meas}^{l})_{1 \leqslant l \leqslant 6}$.

Figure 8 shows snapshots of the action potential distribution on the computational domain for the exact parameters (left), the initial guess parameters (middle) and the estimated parameters (right).
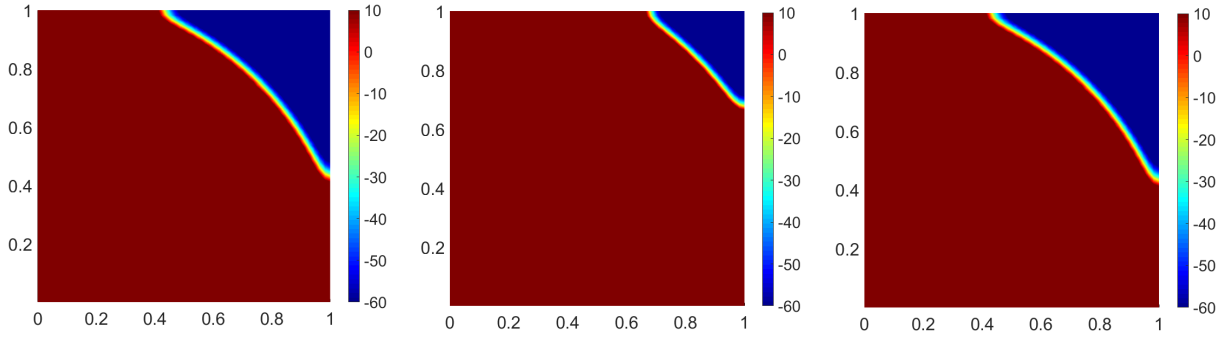
FIGURE 8. 2D visualization of solution v at time $t = 8$msec with exact, guess and optimal parameter values on the left, middle and right respectively.

Figures 9, (respectively, 10 and 11) show the evolution of the parameters $\bar{\varrho}_{Na}$ and $\bar{\varrho}_{si}$ (respectively, $\bar{\varrho}_{K}$, $\bar{\varrho}_{K1}$ and $\bar{\varrho}_{Kp}$, $\bar{\varrho}_{b}$) during the optimization iterations. Results are shown for different levels of noise (0%, 5% and 10%) on the measured data. In each figure, we show the target value of the parameter $\bar{\varrho}_{exact}$ (constant value) and the evolution of the optimized parameters during the iteration.
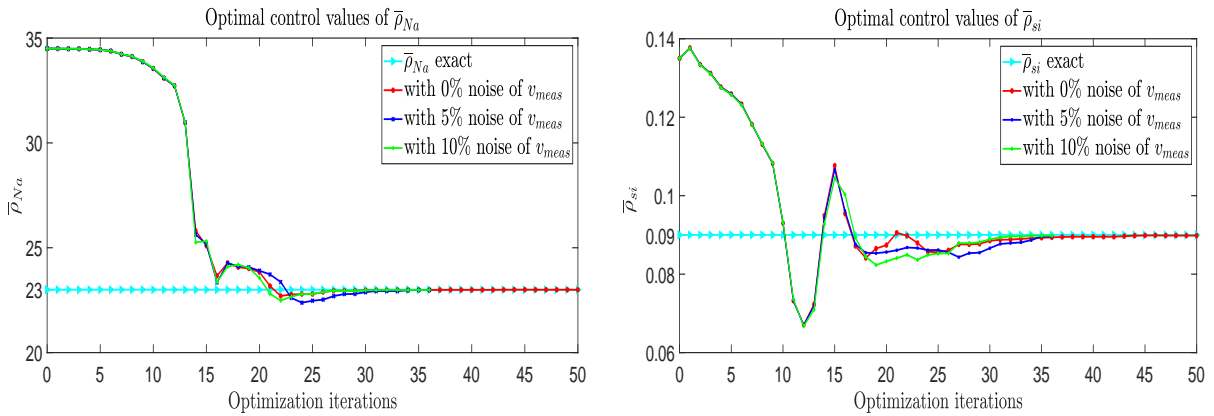

FIGURE 9. The evolution of the optimal control solution $\bar{\varrho}_{Na}$ (left) and $\bar{\varrho}_{si}$ (right) during the optimization iterations.

First, we remark that for all the parameters the optimization algorithm converges to the desired value. We also remark that during the 15 first iteration the evolution of the parameters in the case of noise-free and noisy data was almost the same. Later in the iterations the noise has an effect on the parameters values. We also remarked that with 5 and 10% of noise on the measured data, the optimization algorithm stops at the 35th iteration because it couldn't improve anymore the cost function, while for the noise free case the cost function achieves 10^{-8}.
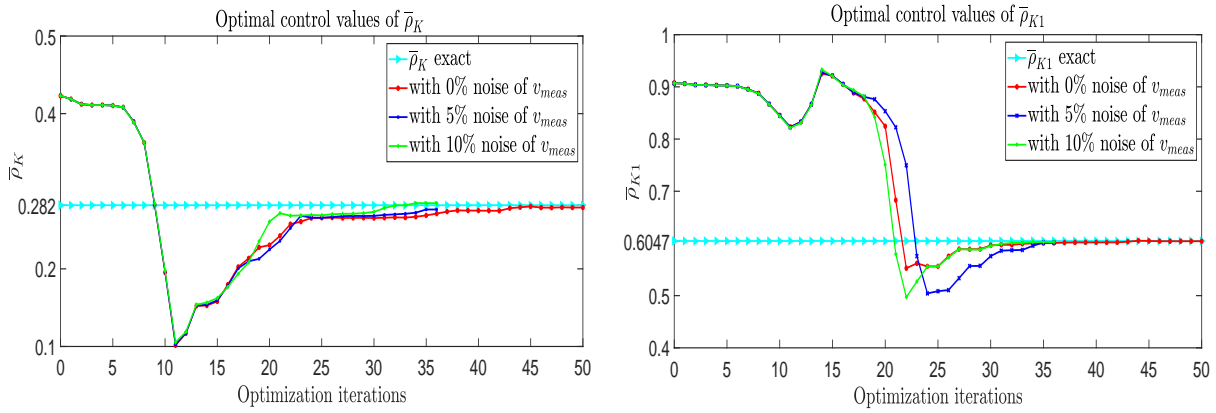

FIGURE 10. The evolution of the optimal control solution $\bar{\varrho}_K$ (left) and $\bar{\varrho}_{K1}$ (right) during the optimization iterations.
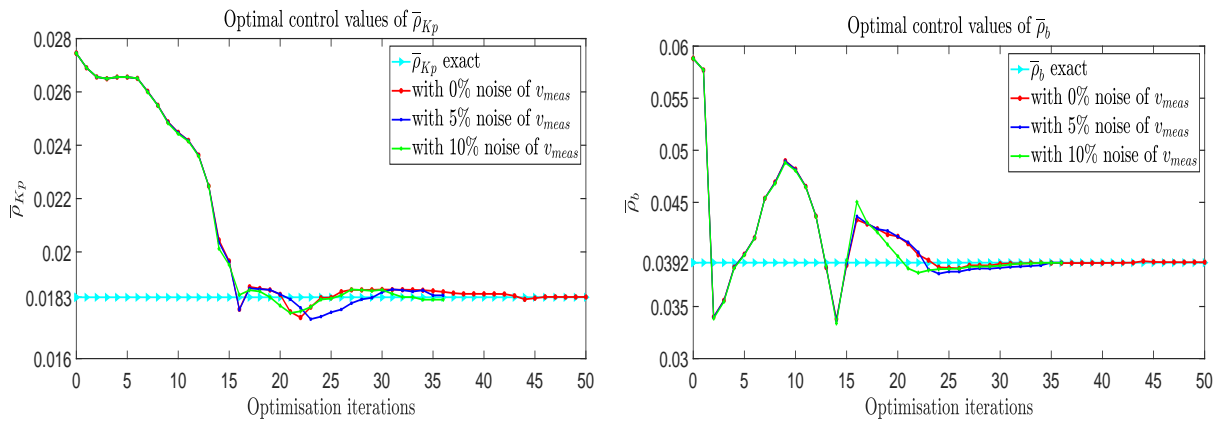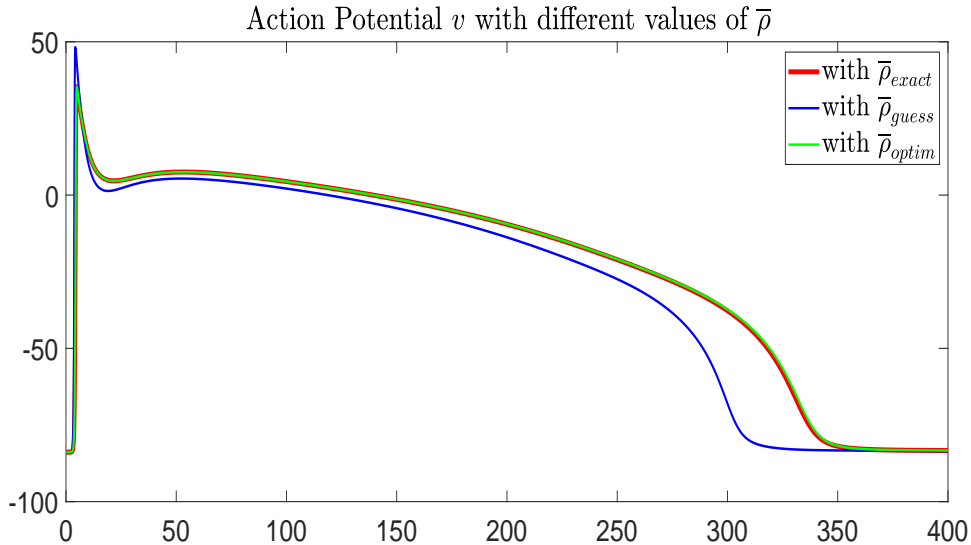

FIGURE 11. The evolution of the optimal control solution $\bar{\varrho}_{Kp}$ (left) and $\bar{\varrho}_b$ (right) during the optimization iterations.

FIGURE 12. Action potential v with different value of $\bar{\varrho}$

6. DISCUSSION AND CONCLUSIONS

In this paper, we presented an original approach for the estimation of maximal conductance parameters in the multi-scale cardiac electrophysiology modelling. We used the bidomain system coupled to the physiological Luo Rudy phase I ionic model. We formulated the parameter estimation problem as an optimization procedure in an optimal control problem where the cost function represents the misfit between the measured action potential and the solution of the bidomain model. There are two results in this work. The first part is related to the mathematical analysis of the maximal conductance parameters estimation. Our result is a proof of the existence of a minimizer of the cost function. The proof is inspired from the work of Yan and Veneziani [46] who proved the existence of the conductivity parameters estimation solution. The second part is related to the numerical estimation of the six conductance parameters introduced in the Luo Rudy phase I ionic model. In order to minimize the cost function, we used a gradient descent method where the gradient is computed by solving an adjoint problem. We detailed the numerical schemes used for the computation of the primal and adjoint problems. Then we conducted different numerical simulation to solve the problem. First, our numerical results show the capability of this approach to estimate separately each of the maximal conductance parameters with a single observation of the action potential in the computational domain. Second, our attempts to solve the optimization problem for multiple parameters estimation using a single measurement failed. Third, using a strategy of multiple observations generated by variating the position of the stimuli in the computational domain, the optimization algorithm were able to converge to the desired parameters with a very satisfactory accuracy. This study shows also that the optimization procedure is robust with respect of noise. Results show that by adding different levels of noise (0%, 5% and 10%), the error on the estimated conductances was less than 2% in the three cases and for all parameters. The challenge is to explore the capability of this method to estimate these physiological parameters when dealing with real life measurement. Finally, we have to say that this study is preliminary and that we didn't explore

all of the potential of the optimal control approach. The method here presented allows the estimation of space dependent parameters. This would be subject of our future research.

REFERENCES

[1] Y. Abidi, M. Bellassoued, M. Mahjoub, and N. Zemzemi. On the identification of multiple space dependent ionic parameters in cardiac electrophysiology modelling. *Inverse Problems*, 34(3):035005, 2018.

[2] Y. Abidi, M. Bellassoued, M. Mahjoub, and N. Zemzemi. Ionic parameters identification of an inverse problem of strongly coupled pdes system in cardiac electrophysiology using carleman estimates. *Mathematical Modelling of Natural Phenomena*, 14(2):202, 2019.

[3] R.A. Adams and J. JF. Fournier. *Sobolev spaces*, volume 140. Elsevier, 2003.

[4] B. Ainseba, M. Bendahmane, and R. Ruiz-Baier. Analysis of an optimal control problem for the tridomain model in cardiac electrophysiology. *Journal of Mathematical Analysis and Applications*, 388(1):231 – 247, 2012.

[5] B. E. Ainseba, M. Bendahmane, and H. Yuan. Stability of conductivities in an inverse problem in the reaction-diffusion system in electrocardiology. *American Institute of Mathematical Sciences*, 10(2):369–385, 2015.

[6] Diego Álvarez, Felipe Alonso-Atienza, José Luis Rojo-Álvarez, Arcadi García-Alberola, and Miguel Moscoso. Shape reconstruction of cardiac ischemia from non-contact intracardiac recordings: A model study. *Mathematical and Computer Modelling*, 55(5-6):1770–1781, 2012.

[7] B. Andreianov, M. Bendahmane, A. Quarteroni, and R. Ruiz-Baier. Solvability analysis and numerical approximation of linearized cardiac electromechanics. *Math. Models Methods Appl. Sci.*, 25(5):959–993, 2015.

[8] G. W. Beeler and H. Reuter. Reconstruction of the action potential of ventricular myocardial fibres. *The Journal of Physiology*, 268(1):177–210, 1977.

[9] M. Bendahmane, N. Chamakuri, E. Comte, and B. Ainseba. A 3d boundary optimal control for the bidomain-bath system modeling the thoracic shock therapy for cardiac defibrillation. *Journal of Mathematical Analysis and Applications*, 437(2):972 – 998, 2016.

[10] E. Beretta, C. Cavaterra, M. C. Cerutti, A. Manzoni, and L. Ratti. An inverse problem for a semilinear parabolic equation arising from cardiac electrophysiology. *Inverse Problems*, 33(10), 2017.

[11] M. Boulakia and E. Schenone. Stability estimates for some parameters of a reaction-diffusion equation coupled with an ode. *Applicable Analysis*, 96(7):1138–1145, 2017.

[12] J. Bouyssier and N. Zemzemi. Parameters estimation approach for the mea/hipsc-cm asaays. In *2017 Computing in Cardiology (CinC)*, pages 1–4. IEEE, 2017.

[13] A. J. Brandao, E. Fernandez-Cara, P. Magalhaes, and M. A. Rojas-Medar. Theoretical analysis and control results for the fitzhugh-nagumo equation. *Electronic Journal of Differential Equations (EJDE)[electronic only]*, 2008:Paper–No 164, 2008.

[14] E. Casas, C. Ryll, and F. Tröltzsch. Sparse optimal control of the schlögl and fitzhugh-nagumo systems. *Computational Methods in Applied Mathematics*, 13(4):415–442, 2013.

[15] N. Chamakuri and K. Kunisch. Primal-dual active set strategy for large scale optimization of cardiac defibrillation. *Applied Mathematics and Computation*, 292:178–193, 2017.

[16] N. Chamakuri, K. Kunisch, and G. Plank. Numerical solution for optimal control of the reaction-diffusion equations in cardiac electrophysiology. *Computational Optimization and Applications*, 49(1):149–178, 2011.

[17] N. Chamakuri, K. Kunisch, and G. Plank. Optimal control approach to termination of re-entry waves in cardiac electrophysiology. *Journal of Mathematical Biology*, 67(2):359–388, 2013.

[18] N. Chamakuri, K. Kunisch, and G. Plank. Application of optimal control to the cardiac defibrillation problem using a physiological model of cellular dynamics. *Applied Numerical Mathematics*, 95:130 – 139, 2015.

[19] N. Chamakuri, K. Kunisch, and G. Plank. Pde constrained optimization of electrical defibrillation in a 3d ventricular slice geometry. *International Journal for Numerical Methods in Biomedical Engineering*, 32(4):e02742, 2016.

[20] C. E. Chávez, N. Zemzemi, Y. Coudière, F. Alonso-Atienza, and D. Alvarez. Inverse problem of electrocardiography: Estimating the location of cardiac ischemia in a 3d realistic geometry. In *International Conference on Functional Imaging and Modeling of the Heart*, pages 393–401. Springer, 2015.

[21] L Clerc. Directional differences of impulse spread in trabecular muscle from mammalian heart. *The Journal of physiology*, 255(2):335–346, 1976.

[22] L. P. Endresen, K. Hall, J. S. Hoye, and J. Myrheim. A theory for the membrane potential of living cells. *European Biophysics Journal*, 29(2):90–103, May 2000.

[23] L.C. Evans. *Partial differential equations*. Graduate Studies in Mathematics. American Mathematical Society, 2 edition, 2010.

[24] M. A. Fernández and N. Zemzemi. Decoupled time-marching schemes in computational cardiac electrophysiology and ecg numerical simulation. *Mathematical biosciences*, 226(1):58–75, 2010.

[25] D. D. Francesco and D. Noble. A model of cardiac electrical activity incorporating ionic pumps and concentration changes. *Philosophical Transactions of the Royal Society of London B: Biological Sciences*, 307(1133):353–398, 1985.

[26] E. Grandi, F.S. Pasqualini, and D.M. Bers. A novel computational model of the human ventricular action potential and Ca transient. *Journal of molecular and cellular cardiology*, 48(1):112–121, 2010.

[27] C. S. Henriquez. Simulating the electrical behavior of cardiac tissue using the bidomain model. *Critical reviews in biomedical engineering*, 21(1):1–77, 1993.

[28] A. L. Hodgkin and A. F. Huxley. A quantitative description of membrane current and its application to conduction and excitation in nerve. *The Journal of Physiology*, 117(4):500–544, 1952.

[29] T. J. Hund and Y. Rudy. Rate dependence and regulation of action potential and calcium transient in a canine cardiac ventricular cell model. *Circulation*, 110(20):3168–3174, 2004.

[30] J. P. Keener and J. Sneyd. *Mathematical Physiology, I: Cellular Physiology*. Graduate Studies in Mathematics. Springer-Verlag New York, 2009.

[31] K. Kunisch and M. Wagner. Optimal control of the bidomain system (iii): Existence of minimizers and first-order optimality conditions. *ESAIM: Mathematical Modelling and Numerical Analysis*, 47(4):1077–1106, 2013.

[32] J. Lassoued, M. Mahjoub, and N. Zemzemi. Stability results for the parameter identification inverse problem in cardiac electrophysiology. *Inverse Problems*, 32(11), 2016.

[33] J. L. Lions. *Quelques méthodes de résolution des problemes aux limites non linéaires*. Dunod, 1969.

[34] C. H. Luo and Y. Rudy. A model of the ventricular cardiac action potential: Depolarization, repolarization, and their interaction. *Circulation Research*, 68(6):1501–1526, 1991.

[35] C. H. Luo and Y. Rudy. A dynamic model of the cardiac ventricular action potential. i. simulations of ionic currents and concentration changes. *Circulation Research*, 74(6):1071–1096, 1994.

[36] D. Ngoma, P. Vianney, Y. Bourgault, and H. Nkounkou. Parameter identification for a non-differentiable ionic model used in cardiac electrophysiology. *Applied Mathematical Sciences*, 9(150):7483–7507, 2015.

[37] B. F. Nielsen, M. Lysaker, and A. Tveito. On the use of the resting potential and level set methods for identifying ischemic heart disease: An inverse problem. *Journal of computational physics*, 220(2):772–790, 2007.

[38] D. Noble. Cardiac action and pacemaker potentials based on the hodgkin-huxley equations. *Nature Publishing Group*, 188(4749):495–497, 1960.

[39] P. C. Franzone L. F. Pavarino and S. Scacchi. *Mathematical Cardiac Electrophysiology*. Springer International Publishing, 2014.

[40] D. E. Roberts, L. T. Hersh, and A. M. Scher. Influence of cardiac fiber orientation on wavefront voltage, conduction velocity, and tissue resistivity in the dog. *Circulation research*, 44(5):701–712, 1979.

[41] D. E. Roberts and A. M. Scher. Effect of tissue anisotropy on extracellular potential fields in canine myocardium in situ. *Circulation Research*, 50(3):342–351, 1982.

[42] K. H. W. J ten Tusscher and A. V. Panfilov. Cell model for efficient simulation of wave propagation in human ventricular tissue under normal and pathological conditions. *Phys. Med. Biol.*, 51:6141, 2006.

[43] L. Tung. *A bidomain model for describing ischemic myocardial d-c potentials*. PhD thesis, Massachusetts Institute of Technology, 1978.

[44] M. Veneroni. Reaction-diffusion systems for the macroscopic bidomain model of the cardiac electric field. *Nonlinear Analysis: Real World Applications*, 10:849–868, 2009.

[45] B. Wu, L. Yan, Y. Gao, and Q. Chen. Carleman estimate for a linearized bidomain model in electrocardiology and its applications. *Nonlinear Differential Equations and Applications NoDEA*, 25(1):4, 2018.

[46] H. Yang and A. Veneziani. Estimation of cardiac conductivities in ventricular tissue by a variational approach. *Inverse Problems*, 31(11):115001, 2015.

[1] TUNIS EL MANAR UNIVERSITY, ENIT-LAMSIN, BP 37, LE BELVÉDÈRE 1002 TUNIS, TUNISIA.

E-mail address: yassine.abidi@enit.rnu.tn

E-mail address: moncef.mahjoub@lamsin.rnu.tn

[2] INRIA, BORDEAUX SUD-OUEST, 200 AVENUE DE LA VIELLE TOUR 33405 TALENCE CEDEX FRANCE.
E-mail address: nejib.zemzemi@inria.fr